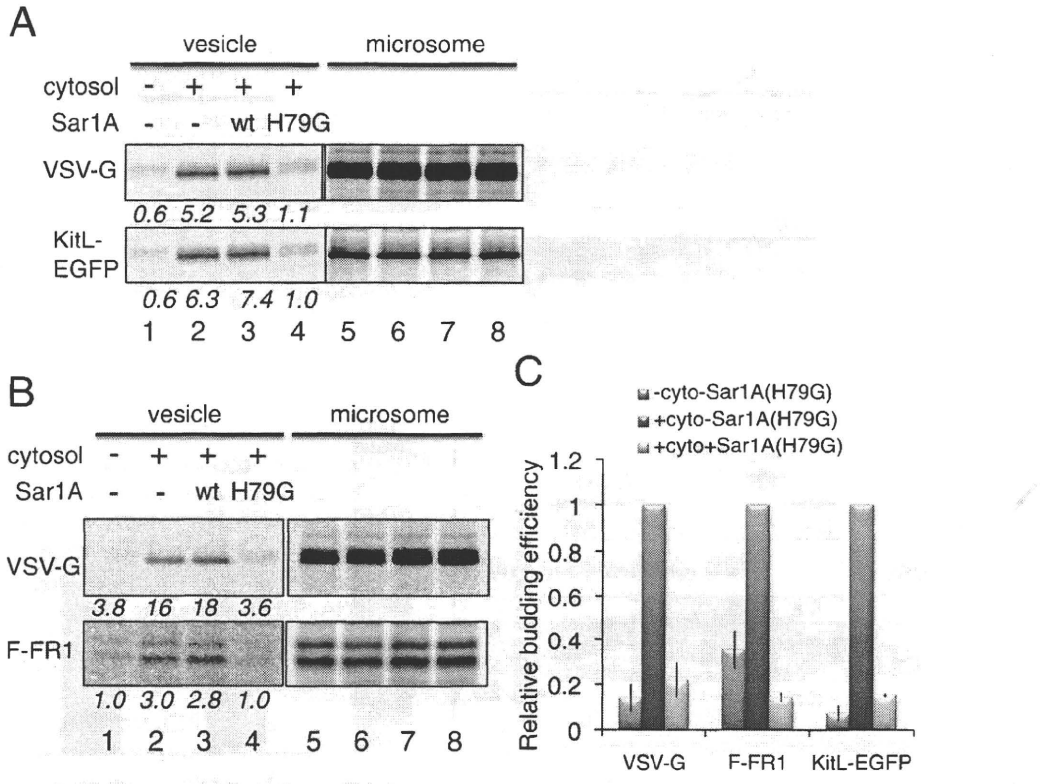

Figure 7: Microsome-based budding assay. ER-derived vesicles were prepared from a microsome fraction derived from pulse-labeled CHO-K1 cells co-expressing (A) KitL-EGFP and VSV-G or (B) F-FR1 and VSV-G. Lanes 1–4, vesicle fractions; lanes 5–8, the remaining microsome fractions. Italic numbers correspond to the percentage of each protein found in the vesicle fraction. (C) Relative budding efficiency of several cargo proteins in microsome-based budding assay. Budding efficiency was normalized to that in the presence of rat liver cytosol alone [+cyto-Sar1A(H79G)]. $n = 9$, $n = 4$ and $n = 2$ for VSV-G, F-FR1 and KitL-EGFP, respectively.

We found no evidence from *in vivo* pulse-chase experiments with yeast cells that Sar1p was less required for ER-to-Golgi transport of GPI-APs than for ER-to-Golgi transport of other secretory proteins. In pulse-chase experiments, we saw no vacuolar form of CPY in *sar1E112K* mutant cells even though the ER-to-Golgi transport of CPY was partially functional according to the appearance of the Golgi form at early chase time-points (Figure 4A–C). In wild-type cells, transport from the Golgi to the vacuole is certainly not rate limiting. We conclude that this *sar1* mutant has a severe defect in Golgi-to-vacuole transport *in vivo*. Because there is no evidence for a direct function of Sar1p in Golgi-to-vacuole transport we conclude that we cannot differentiate between direct and indirect effects of the *sar1* mutation *in vivo* and therefore this mutant does not allow us to confirm our biochemical findings *in vivo*. This apparent discrepancy between the *in vitro* and *in vivo* requirement of yeast GPI-APs for Sar1p might be also explained if vesicles containing GPI-APs produced with reduced Sar1p activity are not fully functional for fusion with *cis*-Golgi *in vivo*. For example, by using the *in vitro ER* budding assay, we found that incorporation of the SNAREs Bos1p and Sec22p into the vesicles was significantly reduced in the presence of Sar1(H77L) (Figure 4D) under conditions where incorporation of yeast GPI-APs into vesicles was only partially affected (Figure 3A,B). These findings imply that the ER-derived vesicles containing GPI-APs produced when the activity of Sar1p is reduced might not contain sufficient SNARE molecules required for their fusion with *cis*-Golgi apparatus *in vivo*. In the same assay, we also found that the COPII component Sec23p was recovered in the vesicle fraction only in the presence of the GTP-locked form of Sar1(H77L) (Figure 4D). COPII vesicles must disassemble their coats before fusing with the Golgi apparatus and this uncoating seems to be mediated by GTP hydrolysis by Sar1 (46). These results might explain the difference in the Sar1p requirement of yeast GPI-APs seen *in vivo* in the ER-to-Golgi transport assay and *in vitro* in the ER budding assay.

Several requirements for the ER exit of GPI-APs are shared between yeast and mammalian cells. Efficient ER exit of GPI-APs depends on proper anchorage to GPI (6–8,47) and modifications of the glycan part of GPI in the ER such as inositol deacylation mediated by PGAP1/yeast BST1 (48) and removal of ethanolamine-phosphate attached to the second mannose mediated by PGAP5/yeast TED1 (49,50). Another common feature is

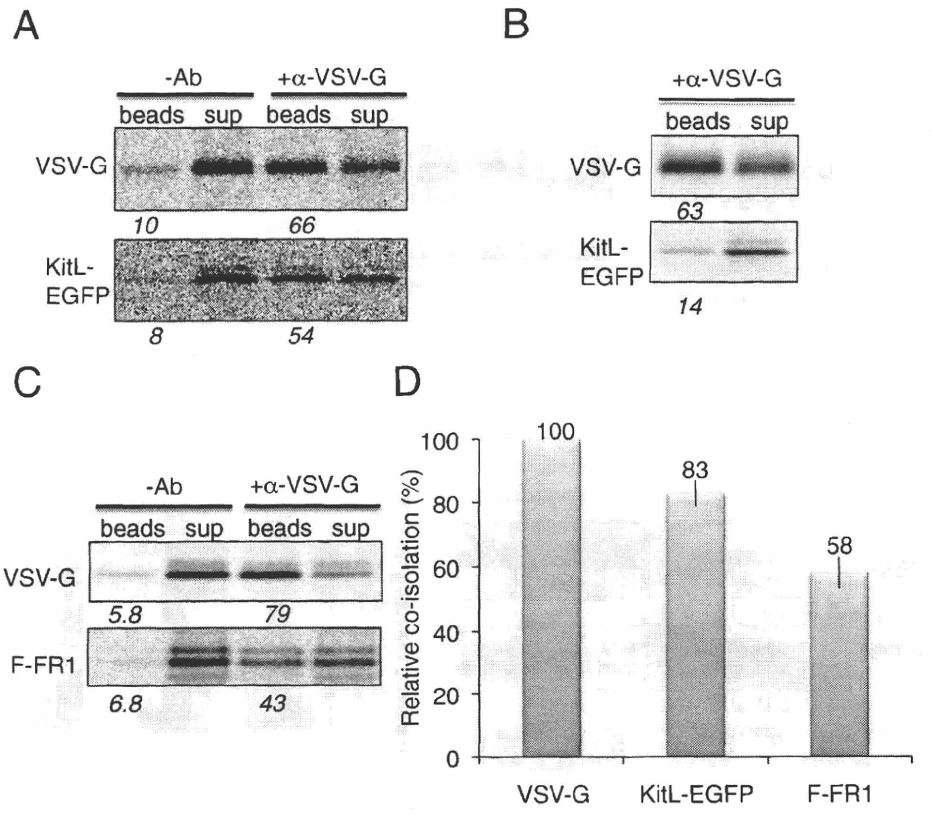

Figure 8: Sorting and tethering/fusion assays. Immunoisolation was done with protein G–Sepharose pre-bound with anti-VSV-G antibody (+α-VSV-G) or mock treated (–Ab) with a vesicle fraction produced *in vitro* by using (A) a microsome fraction from CHO-K1 cells co-expressing KitL-EGFP and VSV-G or (B) mixed microsome fractions prepared separately from CHO-K1 cells expressing either KitL-EGFP or VSV-G. (C) Immunoisolation was done with protein G–Sepharose pre-bound with anti-VSV-G antibody (+α-VSV-G), or mock treated (–Ab) mixed with a vesicle fraction produced *in vitro* by using a microsome fraction from CHO-K1 cells co-expressing F-FR1 and VSV-G. (D) Quantification of A and C as in Figure 6B. $n = 2$ for KitL-EGFP, $n = 4$ for F-FR1. The immunoisolation efficiency of VSV-G varied from 50 to 79%.

the need for members of the p24 protein family (51,52). The p24 single-span transmembrane proteins have been proposed to act as an ER exit receptor for luminal GPI-APs (53). This protein family seems to be involved in various stages of the secretory pathway including bidirectional transport between the ER and the Golgi apparatus and the post-Golgi pathway (54), but the precise role of the p24 protein family for transport of GPI-APs remains elusive.

There are also several differences in how GPI-APs exit the ER in mammalian cells and yeast. GPI-APs show different degrees of Sar1 requirement for ER exit *in vitro*. So far, several non-exclusive roles for Sar1 have been postulated. In principle, the activated GTP-bound form of Sar1 recruits the Sec23–Sec24 protein complex by binding to Sec23, and cargo proteins are then recruited by binding to Sec24 to form the prebudding complex (1). In some cases, as for VSV-G, activated GTP-Sar1 binds directly to the cytoplsmic tail of VSV-G. This interaction promotes the binding of Sec23–Sec24 to VSV-G via its ER exit signal (55). It was also proposed that the Sar1 GTPase cycle might be actively involved in concentrating cargo proteins in COPII vesicles based on the observation that a kinetically stable prebudding complex undergoes multiple rounds of the Sar1 GTPase cycle (56). Finally, Sar1 might also regulate the fission step of COPII vesicles (31,57). Some transmembrane secretory proteins must bind directly to Sar1p in order to be recruited efficiently into a prebudding complex and continuous Sar1 GTPase cycles contribute to their concentration in COPII vesicles. Yeast GPI-APs, by contrast, might have an intrinsic ability to concentrate into ER subdomains by interactions between a properly remodeled GPI-lipid moiety and ceramide, both of which contain the saturated long-chain C26 fatty acid. Therefore, the Sar1-dependent concentration mechanism might no longer be required for yeast GPI-APs. These two types of concentration mechanisms might also explain protein sorting upon ER exit in yeast (18). Alternatively, considering the role in vesicle fission of Sar1, yeast ER subdomains containing high concentrations of GPI-APs and ceramide might more easily pinch-off from the ER

than the COPII-mediated prebudding complexes when functional Sar1 protein is limiting.

In mammalian cells, in contrast to yeast, the GPI-lipid remodeling required for incorporation into DRM *in vitro* likely occurs only after arrival of the protein at the Golgi apparatus (11,12). We confirmed that accumulation of Venus-CD59 at ERES was not affected in cells defective in GPI-lipid remodeling [PGAP2(−) cells; R. Watanabe, unpublished data]; therefore, mammalian GPI-APs in the ER might not display such intrinsic ability to concentrate in particular ER subdomains but, instead, they may rely fully on the COPII machinery, as do transmembrane secretory proteins. This hypothesis is consistent with the fact that ongoing sphingolipid biosynthesis is important for ER-to-Golgi transport of GPI-APs in yeast but not in mammalian cells. The lack of striking segregation of GPI-APs and secretory transmembrane proteins upon ER exit in mammalian cells agrees well with our finding that they are similar in their dependence upon Sar1 for incorporation into vesicles. Of course, our result does not rule out the possibility that some endogenous GPI-APs might still be sorted from transmembrane secretory proteins in mammalian cells.

Several reports suggest that GPI-APs are sorted from other secretory transmembrane proteins at the Golgi apparatus in mammalian cells (58) and this sorting is likely mediated by interaction of GPI-APs with sphingolipid-enriched membranes [so-called lipid rafts (14,59)]. The inhibition of sphingolipid biosynthesis affects apical targeting of GP-2, a GPI-AP, in MDCK cells (60). We postulate that the sphingolipid- and GPI-lipid-moiety-dependent GPI-AP sorting from other secretory proteins that happens upon ER exit in yeast cells occurs instead in the Golgi apparatus in mammalian cells because of the different localization of the remodeling enzymes. It will be interesting to test whether the lack of GPI remodeling affects transport kinetics and apical sorting of GPI-APs in polarized epithelial cells.

Finally, one might wonder why the functional association of GPI-APs and sphingolipid begins at different stages along the secretory pathway in the two organisms. In yeast, ER-to-Golgi transport of ceramide occurs by both a vesicular and a non-vesicular pathway (61–63). Furthermore, ER-to-Golgi transport of GPI-APs and ceramide are tightly coupled (20,21,32,64). In mammalian cells, by contrast, ceramide produced in the ER is mainly transported to the Golgi apparatus by the cytosolic protein CERT (65,66). The reason for this difference could be the chemical nature of the ceramides. The major yeast ceramide has a considerably longer acyl chain than ceramides in animal cells, and CERT is unable to transport these long-chain ceramides (67). Another possible explanation involves the organization of secretory pathway (68,69). In mammalian cells, the Golgi apparatus, composed of several stacks of cisternae, is confined to a perinuclear position, whereas yeast has a dispersed Golgi apparatus with solitary cisternae distributed throughout the cytoplasm (70). *Drosophila melanogaster* imaginal disc cells have individual Golgi stacks distributed throughout the cytoplasm (71). It would be interesting to examine whether GPI-AP sorting from other transmembrane proteins happens in such cells, and if so, which organelle is responsible for the protein sorting.

Materials and Methods

Cells, culture conditions and transfection

The CHO-K1 cell line, GPI biosynthsis defective cell line, M2S2 (37), SPT mutant CHO cell line, LY-B (22) and their transfectants were routinely cultured in Ham's F-12 medium (Sigma) supplemented with 10% fetal bovine serum plus antibiotics. The cells were transfected by electroporation at 260 V and 960 μF in a Gene Pulser (Bio-Rad). The CHO-K1 and LY-B cells constitutively expressing GPI-anchored human PLAP were established as described previously (65).

Antibody and reagents

The rabbit anti-p58 antibody was provided by Prof. J. Saraste (University of Bergen, Bergen, Norway). The mouse monoclonal anti-VSV-G antibodies P5D4 and 172214 were provided by Prof. J. Gruenberg (University of Geneva, Geneva, Switzerland). Rabbit anti-human Sec13, anti-yeast Sec22 and anti-sec23 antibodies were provided by Prof. R. Schekman (University of California, Berkeley, USA). Rabbit anti-KDEL, anti-calnexin and anti-Sec61α antibodies were purchased from Abcam. Rabbit anti-GFP antibody was produced by immunizing rabbits with recombinant GST-Venus protein (a variant of GFP). The SPT inhibitor, myriocin, also known as ISP-1, was purified from the culture broth of the fungus *Isaria sinclairii* (72). Purified α-SNAPL294A was from Prof. J.C. Hay (The University of Montana, Montana, USA).

Plasmids

The following mammalian expression plasmids were provided by others, as indicated: pMD2G-VSVG by Prof. D. Trono (Ecole Polytechnique Fédérale de Lausanne, Lausanne, Switzerland), KitL-EGFP-wt and KitL-EGFP-d36 (36) by Dr. B. Wehrle-Haller (University of Geneva, Geneva, Switzerland), pME-puro-FLAG-FR1, pME-FLAG-CD59-GPI and pME-puro-FLAG-CD59 by Prof. T. Kinoshita (Research Institute for Microbial Diseases, Osaka University, Osaka, Japan) and LDLR-EGFP by Prof. G. Kreitzer (Weill-Cornell Medical College, New York, USA). To construct pME-puro-Venus-FLAG-CD59, the ORF of VENUS was amplified by PCR with pBS7 (Yeast Resource Center) by using upper and lower primers both containing SbfI sites and integrated into the pME-puro-FLAG-CD59 at the SbfI site in the plasmid. To construct pME-mCherry-FLAG-CD59-GPI, the ORF of mCherry was amplified by PCR with pBS35 (Yeast Resource Center) by using upper and lower primers both containing NsiI sites and integrated into the pME-FLAG-CD59-GPI at SbfI site. Plasmids for recombinant hamster wild-type Sar1A (pJK1), Sar1AH79G (pJK2) and Sar1AT39N (pJK3) were provided by Prof. R. Schekman (University of California, Berkeley, USA). To construct pGEX-yeast Sar1H77L, the ORF of yeast Sar1H77L, obtained from Prof. A. Nakano (RIKEN Discovery Research Institute, Saitama, Japan), was amplified by polymerase chain reaction (PCR) by using an upper primer containing BamHI and a lower primer containing NotI and integrated into the pGEX4T-3 vector at BamHI and NotI sites. The plasmids for recombinant mutant alpha-toxins were from Prof. T. Kinoshita and Prof. Y. Hong (Chonnam National University, Gwangju, Korea). The sequences were verified for all plasmids constructed in this study.

Pulse-chase experiment

Wild-type CHO-K1 and mutant LY-B cell transfectants expressing PLAP were cultured in Nutridoma-BO medium (Ham's F-12 medium containing

1% Nutridoma-SP (Roche Applied Science), 0.1% fetal bovine serum and 10 μM sodium oleate–bovine serum albumin (BSA) complex plus antibiotics for two days before the experiment to deplete exogenous sphingolipids from the normal medium. The pulse-chase experiments followed by Endo H treatment were performed as described previously (65).

Lipid analysis

Quantification of lipids was done as previously (22).

Metabolic labeling

Transfectants were cultured in 14-cm dishes after electroporation. After 24 h, they were preincubated with DMEM lacking L-methionine and L-cysteine for 30 min and then pulsed with 100 μCi/mL ^{35}S-methionine and ^{35}S-cysteine (Easy Tag Expre35s35s, Perkin Elmer) for 30 min. After the pulse-labeling, cell metabolism was immediately stopped by addition of 10 mM NaF/NaN_3.

The semi-intact cell in vitro budding assay

Semi-intact cells were prepared as described previously with minor modifications (28,73). Briefly, 80–90% confluent pulse-labeled cells (growing in 14-cm culture dishes) were harvested with trypsin–ethylenediaminetetraacetic acid (EDTA). After inactivating the trypsin with soybean trypsin inhibitor, the cells were suspended in 8 mL of ice-cold B88-0 (20 mM HEPES pH 7.2, 250 mM Sorbitol, 150 mM KOAc). The plasma membrane was permeabilized by incubating for 5 min on ice with 16 μL of 20 mg/mL digitonin stock in DMSO (final concentration 40 μg/mL). To stop permeabilization and remove the detergent, the cell suspension was diluted by addition of 11 mL B88-0 and centrifuged at 1000 × *g* for 3 min at 4°C. The pellet was washed once with B88-0, resuspended in 200 μL of B88-0 and kept at −80°C. After thawing on ice, semi-intact cells were washed twice with B88 (B88-0 supplemented with 5 mM $Mg(OAc)_2$) plus protease inhibitors (10 μg/mL leupeptin, 5 μg/mL pepstatin A, 2 μg/mL aprotinin) and used for *in vitro* assays.

The *in vitro* COPII vesicle formation assay (100 μL) was carried out in B88 plus protease inhibitors supplemented with 1.5 mM ATP, 60 mM creatine phosphate, 20 unit/mL creatine phosphokinase, 0.5 mM GTP plus semi-intact cells and 6–8 mg/mL rat liver cytosol prepared as described previously (74), with or without recombinant Sar1 protein (10 μg/mL) prepared as described previously (75), at 25°C for 60 min. Small aliquots were taken to estimate incorporation efficiency before incubation. The reaction mixture was centrifuged at 14 000 × *g* for 10 minutes at 4°C and the 14K supernatant (70 μL) was collected and further centrifuged at 100 000 × *g* for 20 min at 4°C to obtain the vesicle fraction. For analysis of cargo proteins, fractions were either solubilized with VSV-G buffer (10 mM Tris–HCl pH 7.4, 150 mM NaCl, 1 mM EDTA, 1% Nonidet P40, 1 mg/mL BSA) plus protease inhibitors and immunoprecipitated with anti-VSV-G and anti-GFP antibodies plus protein A/G-Sepharose (GE Healthcare) or solubilized with RIPA buffer (50 mM Tris–HCl pH 7.5, 150 mM NaCl, 1% TX-100, 0.5% DOC, 0.1% SDS) plus protease inhibitors and immunoprecipitated with anti-FLAG-agarose beads. The samples were separated by SDS–PAGE and quantified using a Cyclone Phosphor Imager (Packard). To analyze the ER-resident proteins calnexin and Sec61α, the vesicle and total fractions were separated by SDS–PAGE and immunoblotted with anti-calnexin (1:5000) and anti-Sec61α (1:2500) antibodies.

The yeast in vitro budding assay and pulse-chase experiments

The yeast ER budding assay was performed as described previously (18,32). Recombinant wild-type and mutant yeast Sar1p were added at 7 μg/mL during the budding assay. In pulse-chase experiments using wild-type (RH2874) and mutant *sar1E112K* (TOY225) (34) yeast strains, cells were preincubated at the indicated temperature for 15 min, then labeled and chased for various times. Total cell extracts were processed for immunoprecipitation with anti-Gas1p (GPI-AP) or anti-CPY (soluble protein) antibodies.

Fluorescence microscopy of cargo proteins in the ERES

Transfectant cells were cultured for two days on acid-washed 12-mm-diameter glass coverslips at 37°C. After incubating at 10°C for 1–2 h in Ham's F-12 medium supplemented with 10 % fetal bovine serum, antibiotics and 20 mM HEPES–HCl pH 7.4, the cells were washed twice with PBS containing Ca^{2+} and Mg^{2+}, PBS(+), fixed in 4% paraformaldehyde in PBS for 8 min, then washed three times with 10 mM glycine in PBS(+) to block residual paraformaldehyde. The cells were permeabilized and blocked with 3% BSA in PBS (+) containing 0.05% (w/v) saponin for 30 min at room temperature. After washing with 0.1% BSA in PBS (+), the cells were incubated with anti-Sec13 antibody (1:10000) in 1% BSA in PBS (+) for 1 h. After washing three times with 0.1% BSA in PBS (+), the cells were incubated with Cy5-conjugated anti-Rabbit IgG (1:200) (Jackson immunoResearch) in 1% BSA in PBS (+) for 1 h. After washing three times with 0.1% BSA in PBS (+), the coverslips were mounted in Prolong Gold antifade reagent (Invitrogen). To visualize internal Venus-CD59 and mCherry-CD59 signals, the cells were washed with Opti-MEM twice and incubated with 0.3 unit/mL PI-PLC (Invitrogen) in Opti-MEM at 37°C for 40 min, and this was followed by incubation at 10°C in Ham's F-12 medium and processing as described above. Micrographs were acquired with a 100× 1.4 numerical aperture oil objective lens with an AXIOZ1 microscope and an AxioCam MRm charge-coupled device camera controlled by the software AxioVisionRel.4.6 (all from Zeiss). The data were processed with ImageJ software. Where colocalization efficiencies were measured, micrographs were analyzed with Imaris software to detect the dots corresponding to cargo accumulation and ERES in each channel. The overlapping dots were counted manually.

Immunoisolation of in vitro produced COPII vesicles

A bed volume of 35 μL protein G–Sepharose 4 Fast Flow was used for each immunoisolation; this was washed twice with 5% BSA (A3803 Sigma) in PBS and incubated with 5% BSA in PBS with or without anti-P5D4 or anti-GFP antibodies for 5 h. The antibody-coated protein G beads were washed twice with 5% BSA in PBS and used for immunoisolation of vesicles. The 14K supernatant fraction from *in vitro* budding assays was diluted with four volumes of 5% BSA in PBS and incubated with the antibody-coated protein G beads overnight with gentle agitation. The beads and supernatant were separated by 400 × *g* for 2 min. The supernatant was further centrifuged at 60 000 rpm (150 000 × g) for 1 h with TLA100.3 (Beckman). The pellet was solubilized with the appropriate immunoprecipitation buffer. The bead fraction was washed with 0.1% BSA in PBS three times. The proteins collected with the beads were eluted by washing with 2× VSV-G buffer and 100 mM triethylamine pH 12.5, and the pH was adjusted to neutral with 1 M Tris–HCl pH 6.8. The eluate was diluted three times with the appropriate immunoprecipitation buffer. The immunoprecipitation step and subsequent analyses were done as described above. To quantify the percentage of proteins in VSV-G-containing or LDLR-EGFP-containing vesicles, we divided the percentage of individual proteins found in the pellet fraction by the percentage of immunoisolated VSV-G or LDLR-EGFP. This enabled comparison of several independent experiments in which the immunoisolation efficiency can vary.

The microsome-based budding assay

Microsome fractions were prepared as described previously (75,76). Pulse-labeled cells were collected by scraping and cell pellets were kept at −80°C. After thawing on ice, the cells were disrupted by passing through a 22-gauge needle 20 times in Buffer F (10 mM HEPES–KOH at pH 7.2, 250 mM sorbitol, 10 mM KOAc, 1.5 mM $Mg(OAc)_2$) plus protease inhibitors. After centriguging at 1000 × *g* for 5 min to remove nuclei, the supernatant fraction was placed in siliconized microcentrifuge tubes and the microsome fraction was sedimented at 6000 × *g* for 10 min.

After two washes with Buffer E [50 mM HEPES–KOH at pH 7.2, 250 mM sorbitol, 70 mM KOAc, 5 mM potassium EGTA, 2.5 mM $Mg(OAc)_2$ plus protease inhibitors], the microsome pellet was resuspended in Buffer E. The *in vitro* COPII vesicle formation assay (86 µL) was carried out in Buffer E supplemented with 1.5 mM ATP, 60 mM creatine phosphate, 20 unit/mL creatine phosphokinase, 0.5 mM GTP plus microsome fraction and 6–8 mg/mL rat liver cytosol, with or without various recombinant Sar1 proteins (10 µg/mL), at 25°C for 60 min. The reaction mixture was centrifuged at 14 000 × ***g*** for 20 min at 4°C and the 14K supernatant (60 µL) was collected and further centrifuged at 100 000 × ***g*** for 20 min at 4°C to obtain the vesicle fraction. The rest of the reaction mixture (total fraction) was used to measure incorporation efficiency. The vesicle and total fractions were analyzed as described above.

Acknowledgments

We are grateful for the generous gifts of plasmids, cell lines, antibodies and reagents from J. Gruenberg, J.C Hay, Y. Hong, T. Kinoshita, G. Kreitzer, A. Nakano, H. Riezman, J. Saraste, R. Schekman, D. Trono, R. Tsien and B. Wehrle-Haller. The study was initiated in H. Riezman's laboratory. We also thank C. Bauer and J. Bosset from the Bioimaging Platform of NCCR Frontiers in Genetics for their technical help. We thank members of our department, particularly H. Riezman, J. Gruenberg and T. Soldati, for their critical comments and discussions. This study was supported by the Swiss National Science Foundation through a Marie Heim-Vögtlin fellowship (R.W), research grants (H. Riezman and R.W.) and an SNF professorship (R.W).

Supporting Information

Additional Supporting Information may be found in the online version of this article:

Figure S1: Biochemical analyses of exogenously expressed cargo proteins in CHO-K1 cells. (A) The expression level of the exogenous GPI-APs was comparable to that of an unknown endogenous GPI-AP in CHO-K1 cell. Two different recombinant mutant alpha-toxins described previously (1,2) were used to detect exogenous and endogenous GPI-APs expressed in CHO-K1 cells. Both mutant alpha-toxins contained point mutations that substantially reduce cytotoxity but retain binding activity for GPI-APs. Pulse-labeled CHO-K1 cells expressing F-FR1 and F-CD59 were lysed with RIPA buffer and the lysates were mixed with glutathione–Sepharose beads bound to either recombinant GST-tagged mutant alpha-toxin (R398G; lane 1) or GST (lane 2) or with Ni-NTA–agarose bound to recombinant mutant EGFP and His-tagged alpha-toxin (S189C/S238C; lane 3) or GST (lane 4). The bound samples were separated by SDS–PAGE and quantified by using a Cyclone Phosphor Imager (Packard). In addition to F-FR1 (around 40 kDa) and F-CD59 (around 20 kDa), which are exogenously expressed GPI-APs, a protein band around 60–70 kDa (indicated by arrow) was precipitated specifically by differentially tagged alpha-toxins. The data demonstrate that there is at least one unknown endogenous GPI-AP expressed at similar level as the exogenous GPI-APs.

(B and C) Kinetics of transport of F-FR1, F-CD59 and VSV-G from the ER to the Golgi apparatus in CHO-K1 cells. CHO-K1 cells expressing F-FR1, F-CD59 and VSV-G were pulsed for 30 min with ^{35}S-Met and ^{35}S-Cys and chased for the indicated times. Immunoprecipitates were untreated (–) or treated with Endo H (+) for 16 h and then separated by SDS–PAGE. R, Endo H-resistant form; S, Endo H-sensitive form; C, cleaved form by Endo H (B). (C) Quantification of B. (D) Microsome-based budding assay. Immunoblotting of endogenous p58/rat ERGIC-53 (a protein that recycles between the ER and Golgi apparatus) and GRP78 (an ER-resident protein) in the vesicle fractions (lanes 1–5) and in 20% of the remaining microsome fraction (lanes 6–10) produced after incubating microsomes with or without various Sar1A wild-type (wt) and mutant (H79G and T39N) proteins. Arrows indicate the proteins of interest. The p58 protein is incorporated into vesicle fractions in a cytosol-dependent manner and incorporation is inhibited by the addition of mutant Sar1A proteins but not wild-type Sar1A. Italic numbers correspond to the percentage of p58 found in the vesicle fraction. For GRP78, the bands seen at around 78 kDa in the vesicle fractions were too faint to be quantified; however, their intensities were not changed drastically by the presence of different Sar1A mutant proteins and a similar faint band was observed in the vesicle fraction prepared with cytosol alone without donor microsomes (data not shown), suggesting that this signal was partly because of a cytosol contaminant.

Figure S2: Subcellular localization of KitL-EGFP and its mutant KitL-EGFP(delV) at 37 and 10°C. CHO-K1 cells (A) expressing KitL-EGFP at 37°C, (B) expressing KitL-EGFP(delV) at 37°C and (C) after 2 h at 10°C. The black arrows indicate ERES that did not colocalize with cargo proteins. Scale bar, 10 µm.

Figure S3: Localization of Venus-CD59 or mCherry-CD59 at 37 and 10°C. (A) CHO-K1 expressing Venus-CD59 at 37°C. (B) CHO-K1 expressing Venus-CD59 treated with PI-PLC. (C) CHO-K1 expressing Venus-CD59 treated with PI-PLC and incubated at 10°C for 1 h in the presence of 1 mM DTT. (D) CHO-K1 co-expressing Venus-CD59 and mCherry-CD59. The white and black arrows indicate ERES that colocalized or did not colocalize with cargo proteins, respectively. Scale bar, 10 µm.

Figure S4: Localization of Venus-CD59 and KitL-EGFP in GPI-negative CHO-K1 cells at 37 and 10°C. GPI-negative CHO-K1 cells expressing Venus-CD59 at 37°C (A) or at 10°C (B). GPI-negative CHO-K1 cells expressing KitL-EGFP at 37°C (C) or at 10°C (D). The white and black arrows indicate ERES that colocalized or did not colocalize with cargo proteins, respectively. Scale bar, 10 µm.

Please note: Wiley-Blackwell are not responsible for the content or functionality of any supporting materials supplied by the authors. Any queries (other than missing material) should be directed to the corresponding author for the article.

References

1. Lee MC, Miller EA, Goldberg J, Orci L, Schekman R. Bi-directional protein transport between the ER and Golgi. Annu Rev Cell Dev Biol 2004;20:87–123.
2. Leidich SD, Drapp DA, Orlean P. A conditionally lethal yeast mutant blocked at the first step in glycosyl phosphatidylinositol anchor synthesis. J Biol Chem 1994;269:10193–10196.
3. Kawagoe K, Kitamura D, Okabe M, Taniuchi I, Ikawa M, Watanabe T, Kinoshita T, Takeda J. Glycosylphosphatidylinositol-anchor-deficient mice: implications for clonal dominance of mutant cells in paroxysmal nocturnal hemoglobinuria. Blood 1996;87:3600–3606.
4. Pittet M, Conzelmann A. Biosynthesis and function of GPI proteins in the yeast Saccharomyces cerevisiae. Biochim Biophys Acta 2007;1771:405–420.
5. Kinoshita T, Fujita M, Maeda Y. Biosynthesis, remodelling and functions of mammalian GPI-anchored proteins: recent progress. J Biochem 2008;144:287–294.
6. Moran P, Caras IW. Proteins containing an uncleaved signal for glycophosphatidylinositol membrane anchor attachment are retained in a post-ER compartment. J Cell Biol 1992;119:763–772.
7. Delahunty MD, Stafford FJ, Yuan LC, Shaz D, Bonifacino JS. Uncleaved signals for glycosylphosphatidylinositol anchoring cause retention of precursor proteins in the endoplasmic reticulum. J Biol Chem 1993;268:12017–12027.
8. Field MC, Moran P, Li W, Keller GA, Caras IW. Retention and degradation of proteins containing an uncleaved glycosylphosphatidylinositol signal. J Biol Chem 1994;269:10830–10837.
9. Bosson R, Jaquenoud M, Conzelmann A. GUP1 of Saccharomyces cerevisiae encodes an O-acyltransferase involved in remodeling of the GPI anchor. Mol Biol Cell 2006;17:2636–2645.
10. Fujita M, Umemura M, Yoko-o T, Jigami Y. PER1 is required for GPI-phospholipase A2 activity and involved in lipid remodeling of GPI-anchored proteins. Mol Biol Cell 2006;17:5253–5264.
11. Tashima Y, Taguchi R, Murata C, Ashida H, Kinoshita T, Maeda Y. PGAP2 is essential for correct processing and stable expression of GPI-anchored proteins. Mol Biol Cell 2006;17:1410–1420.

12. Maeda Y, Tashima Y, Houjou T, Fujita M, Yoko-o T, Jigami Y, Taguchi R, Kinoshita T. Fatty acid remodeling of GPI-anchored proteins is required for their raft association. Mol Biol Cell 2007;18:1497–1506.
13. Fujita M, Jigami Y. Lipid remodeling of GPI-anchored proteins and its function. Biochim Biophys Acta 2008;1780:410–420.
14. Simons K, Ikonen E. Functional rafts in cell membranes. Nature 1997;387:569–572.
15. Muniz M, Morsomme P, Riezman H. Protein sorting upon exit from the endoplasmic reticulum. Cell 2001;104:313–320.
16. Morsomme P, Riezman H. The Rab GTPase Ypt1p and tethering factors couple protein sorting at the ER to vesicle targeting to the Golgi apparatus. Dev Cell 2002;2:307–317.
17. Morsomme P, Prescianotto-Baschong C, Riezman H. The ER v-SNAREs are required for GPI-anchored protein sorting from other secretory proteins upon exit from the ER. J Cell Biol 2003;162:403–412.
18. Castillon GA, Watanabe R, Taylor M, Schwabe TM, Riezman H. Concentration of GPI-anchored proteins upon ER exit in yeast. Traffic 2009;10:186–200.
19. Horvath A, Sutterlin C, Manning-Krieg U, Movva NR, Riezman H. Ceramide synthesis enhances transport of GPI-anchored proteins to the Golgi apparatus in yeast. Embo J 1994;13:3687–3695.
20. Sutterlin C, Doering TL, Schimmoller F, Schroder S, Riezman H. Specific requirements for the ER to Golgi transport of GPI-anchored proteins in yeast. J Cell Sci 1997;110:2703–2714.
21. Watanabe R, Funato K, Venkataraman K, Futerman AH, Riezman H. Sphingolipids are required for the stable membrane association of glycosylphosphatidylinositol-anchored proteins in yeast. J Biol Chem 2002;277:49538–49544.
22. Hanada K, Hara T, Fukasawa M, Yamaji A, Umeda M, Nishijima M. Mammalian cell mutants resistant to a sphingomyelin-directed cytolysin. Genetic and biochemical evidence for complex formation of the LCB1 protein with the LCB2 protein for serine palmitoyltransferase. J Biol Chem 1998;273:33787–33794.
23. Kornfeld R, Kornfeld S. Assembly of asparagine-linked oligosaccharides. Annu Rev Biochem 1985;54:631–664.
24. Hanada K, Nishijima M, Fujita T, Kobayashi S. Specificity of inhibitors of serine palmitoyltransferase (SPT), a key enzyme in sphingolipid biosynthesis, in intact cells. A novel evaluation system using an SPT-defective mammalian cell mutant. Biochem Pharmacol 2000;59:1211–1216.
25. Hidari K, Ichikawa S, Fujita T, Sakiyama H, Hirabayashi Y. Complete removal of sphingolipids from the plasma membrane disrupts cell to substratum adhesion of mouse melanoma cells. J Biol Chem 1996;271:14636–14641.
26. Sutterwala SS, Creswell CH, Sanyal S, Menon AK, Bangs JD. De novo sphingolipid synthesis is essential for viability, but not for transport of glycosylphosphatidylinositol-anchored proteins, in African trypanosomes. Eukaryot Cell 2007;6:454–464.
27. Hong Y, Ohishi K, Inoue N, Kang JY, Shime H, Horiguchi Y, van der Goot FG, Sugimoto N, Kinoshita T. Requirement of N-glycan on GPI-anchored proteins for efficient binding of aerolysin but not Clostridium septicum alpha-toxin. EMBO J 2002;21:5047–5056.
28. Plutner H, Davidson HW, Saraste J, Balch WE. Morphological analysis of protein transport from the ER to Golgi membranes in digitonin-permeabilized cells: role of the P58 containing compartment. J Cell Biol 1992;119:1097–1116.
29. Saito K, Chen M, Bard F, Chen S, Zhou H, Woodley D, Polischuk R, Schekman R, Malhotra V. TANGO1 facilitates cargo loading at endoplasmic reticulum exit sites. Cell 2009;136:891–902.
30. Bonifacino JS, Glick BS. The mechanisms of vesicle budding and fusion. Cell 2004;116:153–166.
31. Bielli A, Haney CJ, Gabreski G, Watkins SC, Bannykh SI, Aridor M. Regulation of Sar1 NH2 terminus by GTP binding and hydrolysis promotes membrane deformation to control COPII vesicle fission. J Cell Biol 2005;171:919–924.
32. Watanabe R, Castillon GA, Meury A, Riezman H. The presence of an ER exit signal determines the protein sorting upon ER exit in yeast. Biochem J 2008;414:237–245.
33. Nakano A, Otsuka H, Yamagishi M, Yamamoto E, Kimura K, Nishikawa S, Oka T. Mutational analysis of the Sar1 protein, a small GTPase which is essential for vesicular transport from the endoplasmic reticulum. J Biochem (Tokyo) 1994;116:243–247.
34. Yamanushi T, Hirata A, Oka T, Nakano A. Characterization of yeast sar1 temperature-sensitive mutants, which are defective in protein transport from the endoplasmic reticulum. J Biochem (Tokyo) 1996;120:452–458.
35. Kirk SJ, Ward TH. COPII under the microscope. Semin Cell Dev Biol 2007;18:435–447.
36. Paulhe F, Imhof BA, Wehrle-Haller B. A specific endoplasmic reticulum export signal drives transport of stem cell factor (Kitl) to the cell surface. J Biol Chem 2004;279:55545–55555.
37. Nakamura N, Inoue N, Watanabe R, Takahashi M, Takeda J, Stevens VL, Kinoshita T. Expression cloning of PIG-L, a candidate N-acetylglucosaminyl-phosphatidylinositol deacetylase. J Biol Chem 1997;272:15834–15840.
38. Tatu U, Braakman I, Helenius A. Membrane glycoprotein folding, oligomerization and intracellular transport: effects of dithiothreitol in living cells. EMBO J 1993;12:2151–2157.
39. Lodish HF, Kong N. The secretory pathway is normal in dithiothreitol-treated cells, but disulfide-bonded proteins are reduced and reversibly retained in the endoplasmic reticulum. J Biol Chem 1993;268:20598–20605.
40. Martinez-Menarguez JA, Geuze HJ, Slot JW, Klumperman J. Vesicular tubular clusters between the ER and Golgi mediate concentration of soluble secretory proteins by exclusion from COPI-coated vesicles. Cell 1999;98:81–90.
41. Stephens DJ, Lin-Marq N, Pagano A, Pepperkok R, Paccaud JP. COPI-coated ER-to-Golgi transport complexes segregate from COPII in close proximity to ER exit sites. J Cell Sci 2000;113:2177–2185.
42. Mezzacasa A, Helenius A. The transitional ER defines a boundary for quality control in the secretion of tsO45 VSV glycoprotein. Traffic 2002;3:833–849.
43. Kreis TE. Microinjected antibodies against the cytoplasmic domain of vesicular stomatitis virus glycoprotein block its transport to the cell surface. EMBO J 1986;5:931–941.
44. Xu D, Hay JC. Reconstitution of COPII vesicle fusion to generate a pre-Golgi intermediate compartment. J Cell Biol 2004;167:997–1003.
45. Bentley M, Liang Y, Mullen K, Xu D, Sztul E, Hay JC. SNARE status regulates tether recruitment and function in homotypic COPII vesicle fusion. J Biol Chem 2006;281:38825–38833.
46. Oka T, Nakano A. Inhibition of GTP hydrolysis by Sar1p causes accumulation of vesicles that are a functional intermediate of the ER-to-Golgi transport in yeast. J Cell Biol 1994;124:425–434.
47. Doering TL, Schekman R. GPI anchor attachment is required for Gas1p transport from the endoplasmic reticulum in COP II vesicles. EMBO J 1996;15:182–191.
48. Tanaka S, Maeda Y, Tashima Y, Kinoshita T. Inositol deacylation of glycosylphosphatidylinositol-anchored proteins is mediated by mammalian PGAP1 and yeast Bst1p. J Biol Chem 2004;279:14256–14263.
49. Haass FA, Jonikas M, Walter P, Weissman JS, Jan YN, Jan LY, Schuldiner M. Identification of yeast proteins necessary for cell-surface function of a potassium channel. Proc Natl Acad Sci U S A 2007;104:18079–18084.
50. Fujita M, Maeda Y, Ra M, Yamaguchi Y, Taguchi R, Kinoshita T. GPI glycan remodeling by PGAP5 regulates transport of GPI-anchored proteins from the ER to the Golgi. Cell 2009;139:352–365.
51. Muniz M, Nuoffer C, Hauri HP, Riezman H. The Emp24 complex recruits a specific cargo molecule into endoplasmic reticulum-derived vesicles. J Cell Biol 2000;148:925–930.
52. Takida S, Maeda Y, Kinoshita T. Mammalian GPI-anchored proteins require p24 proteins for their efficient transport from the ER to the plasma membrane. Biochem J 2008;409:555–562.
53. Muniz M, Riezman H. Intracellular transport of GPI-anchored proteins. EMBO J 2000;19:10–15.
54. Strating JR, Martens GJ. The p24 family and selective transport processes at the ER-Golgi interface. Biol Cell 2009;101:495–509.
55. Aridor M, Fish KN, Bannykh S, Weissman J, Roberts TH, Lippincott-Schwartz J, Balch WE. The Sar1 GTPase coordinates biosynthetic cargo selection with endoplasmic reticulum export site assembly. J Cell Biol 2001;152:213–229.

56. Sato K, Nakano A. Dissection of COPII subunit-cargo assembly and disassembly kinetics during Sar1p-GTP hydrolysis. Nat Struct Mol Biol 2005;12:167–174.
57. Lee MC, Orci L, Hamamoto S, Futai E, Ravazzola M, Schekman R. Sar1p N-terminal helix initiates membrane curvature and completes the fission of a COPII vesicle. Cell 2005;122:605–617.
58. Keller P, Toomre D, Diaz E, White J, Simons K. Multicolour imaging of post-Golgi sorting and trafficking in live cells. Nat Cell Biol 2001;3:140–149.
59. Brown DA, Rose JK. Sorting of GPI-anchored proteins to glycolipid-enriched membrane subdomains during transport to the apical cell surface. Cell 1992;68:533–544.
60. Mays RW, Siemers KA, Fritz BA, Lowe AW, van Meer G, Nelson WJ. Hierarchy of mechanisms involved in generating Na/K-ATPase polarity in MDCK epithelial cells. J Cell Biol 1995;130:1105–1115.
61. Puoti A, Desponds C, Conzelmann A. Biosynthesis of mannosylinositolphosphoceramide in Saccharomyces cerevisiae is dependent on genes controlling the flow of secretory vesicles from the endoplasmic reticulum to the Golgi. J Cell Biol 1991;113:515–525.
62. Reggiori F, Conzelmann A. Biosynthesis of inositol phosphoceramides and remodeling of glycosylphosphatidylinositol anchors in Saccharomyces cerevisiae are mediated by different enzymes. J Biol Chem 1998;273:30550–30559.
63. Funato K, Riezman H. Vesicular and nonvesicular transport of ceramide from ER to the Golgi apparatus in yeast. J Cell Biol 2001;155:949–959.
64. Kajiwara K, Watanabe R, Pichler H, Ihara K, Murakami S, Riezman H, Funato K. Yeast ARV1 is required for efficient delivery of an early GPI intermediate to the first mannosyltransferase during GPI assembly and controls lipid flow from the endoplasmic reticulum. Mol Biol Cell 2008;19:2069–2082.
65. Fukasawa M, Nishijima M, Hanada K. Genetic evidence for ATP-dependent endoplasmic reticulum-to-Golgi apparatus trafficking of ceramide for sphingomyelin synthesis in Chinese hamster ovary cells. J Cell Biol 1999;144:673–685.
66. Hanada K, Kumagai K, Yasuda S, Miura Y, Kawano M, Fukasawa M, Nishijima M. Molecular machinery for non-vesicular trafficking of ceramide. Nature 2003;426:803–809.
67. Kumagai K, Yasuda S, Okemoto K, Nishijima M, Kobayashi S, Hanada K. CERT mediates intermembrane transfer of various molecular species of ceramides. J Biol Chem 2005;280:6488–6495.
68. Prydz K, Dick G, Tveit H. How many ways through the Golgi maze? Traffic 2008;9:299–304.
69. Glick BS, Nakano A. Membrane traffic within the golgi stack. Annu Rev Cell Dev Biol 2009; 25: 113–132.
70. Rossanese OW, Soderholm J, Bevis BJ, Sears IB, O'Connor J, Williamson EK, Glick BS. Golgi structure correlates with transitional endoplasmic reticulum organization in Pichia pastoris and Saccharomyces cerevisiae. J Cell Biol 1999;145:69–81.
71. Yano H, Yamamoto-Hino M, Abe M, Kuwahara R, Haraguchi S, Kusaka I, Awano W, Kinoshita-Toyoda A, Toyoda H, Goto S. Distinct functional units of the Golgi complex in Drosophila cells. Proc Natl Acad Sci U S A 2005;102:13467–13472.
72. Fujita T, Inoue K, Yamamoto S, Ikumoto T, Sasaki S, Toyama R, Chiba K, Hoshino Y, Okumoto T. Fungal metabolites. Part 11. A potent immunosuppressive activity found in Isaria sinclairii metabolite. J Antibiot (Tokyo) 1994;47:208–215.
73. Wilson R, Allen AJ, Oliver J, Brookman JL, High S, Bulleid NJ. The translocation, folding, assembly and redox-dependent degradation of secretory and membrane proteins in semi-permeabilized mammalian cells. Biochem J 1995;307:679–687.
74. Aniento F, Roche E, Cuervo AM, Knecht E. Uptake and degradation of glyceraldehyde-3-phosphate dehydrogenase by rat liver lysosomes. J Biol Chem 1993;268:10463–10470.
75. Kim J, Hamamoto S, Ravazzola M, Orci L, Schekman R. Uncoupled packaging of amyloid precursor protein and presenilin 1 into coat protein complex II vesicles. J Biol Chem 2005;280:7758–7768.
76. Rowe T, Aridor M, McCaffery JM, Plutner H, Nuoffer C, Balch WE. COPII vesicles derived from mammalian endoplasmic reticulum microsomes recruit COPI. J Cell Biol 1996;135:895–911.

Journal of Medical Virology 82:1364–1370 (2010)

Secondary Structure of the Amino-Terminal Region of HCV NS3 and Virological Response to Pegylated Interferon Plus Ribavirin Therapy for Chronic Hepatitis C

Mai Sanjo,[1] Takafumi Saito,[1]* Rika Ishii,[1] Yuko Nishise,[1] Hiroaki Haga,[1] Kazuo Okumoto,[1] Junitsu Ito,[1] Hisayoshi Watanabe,[1] Koji Saito,[1] Hitoshi Togashi,[2] Kazuto Fukuda,[3] Yasuharu Imai,[3] Ahmed El-Shamy,[4] Lin Deng,[4] Ikuo Shoji,[4] Hak Hotta,[4] and Sumio Kawata[1]

[1]*Department of Gastroenterology, Yamagata University School of Medicine, Yamagata, Japan*
[2]*Health Administrative Center, Yamagata University, Yamagata, Japan*
[3]*Division of Gastroenterology, Ikeda Municipal Hospital, Osaka, Japan*
[4]*Division of Microbiology, Kobe University Graduate School of Medicine, Kobe, Japan*

The aim of the study was to identify a predictive marker for the virological response in hepatitis C virus 1b (HCV-1b)-infected patients treated with pegylated interferon plus ribavirin therapy. A total of 139 patients with chronic hepatitis C who received therapy for 48 weeks were enrolled. The secondary structure of the 120 residues of the amino-terminal HCV-1b non-structural region 3 (NS3) deduced from the amino acid sequence was classified into two major groups: A and B. The association between HCV NS3 protein polymorphism and virological response was analyzed in patients infected with group A (n = 28) and B (n = 40) isolates who had good adherence to both pegylated interferon and ribavirin administration (>95% of the scheduled dosage) for 48 weeks. A sustained virological response (SVR) representing successful HCV eradication occurred in 33 (49%) in the 68 patients. Of the 28 patients infected with the group A isolate, 18 (64%) were SVR, whereas of the 40 patients infected with the group B isolate only 15 (38%) were SVR. The proportion of virological responses differed significantly between the two groups ($P < 0.05$). These results suggest that polymorphism in the secondary structure of the HCV-1b NS3 amino-terminal region influences the virological response to pegylated interferon plus ribavirin therapy, and that virus grouping based on this polymorphism can contribute to prediction of the outcome of this therapy. ***J. Med. Virol. 82:1364–1370, 2010.*** © 2010 Wiley-Liss, Inc.

KEY WORDS: hepatitis C; interferon; ribavirin; interaction; polymorphism

INTRODUCTION

Hepatitis C virus (HCV) is the major pathogen that causes chronic liver diseases with a risk of progression to cirrhosis and hepatocellular carcinoma. Currently, the standard treatment for chronic hepatitis C is antiviral therapy using pegylated interferon (Peg-IFN) plus ribavirin (RBV), and this approach is most effective for eradication of HCV viremia. However, even with the widely used treatment regimen of 48 weeks, the rate of sustained virological response (SVR), which indicates eradication of viremia, is still approximately 50% for patients infected with the therapy-resistant HCV genotype 1b (HCV-1b) with a high viral load [Manns et al., 2001; Bruno et al., 2004; Hadziyannis et al., 2004]. It would be useful to predict the virological response to this therapy and to identify patients who would obtain beneficial therapeutic effects before treatment, in order to avoid any serious side effect and to eliminate those who would not be helped by the treatment. In the future it will be important to establish a protocol of tailor-made medicine for chronic hepatitis C.

Grant sponsor: Grant-in-Aid for Scientific Research; Grant number: 21590824; Grant sponsor: Global Center of Excellence program of the Japan Society for the Promotion of Science (Yamagata University School of Medicine and Kobe University Graduate School of Medicine); Grant sponsor: Ministry of Health, Labor and Welfare of Japan.

*Correspondence to: Takafumi Saito, M. D., Department of Gastroenterology, Yamagata University School of Medicine, 2-2-2 Iida-nishi, Yamagata 990-9585, Japan.
E-mail: tasaitoh@med.id.yamagata-u.ac.jp

Accepted 6 March 2010
DOI 10.1002/jmv.21818
Published online in Wiley InterScience (www.interscience.wiley.com)

Both the HCV genotype and pre-treatment viral load are major viral factors that influence the response to IFN-based antiviral therapy, but IFN resistance is also partly due to variation of the amino acid sequence encoded by HCV itself. Enomoto et al. [1996] proposed that variation of 40 amino acids within the NS5A region (aa 2,209–2,248), which is referred to as the IFN sensitivity-determining region (ISDR), is well correlated with IFN responsiveness. ISDR and its adjacent sequence bind and inhibit the enzymatic activity of a double-stranded RNA-activated protein kinase (PKR), which can have an antiviral effect, and therefore the combined region is referred to as the PKR-binding domain (PKR-BD) [Gale et al., 1997, 1998]. A correlation between sequence variation in the PKR-BD and IFN responsiveness has been reported [Nousbaum et al., 2000], and some reports show a correlation between IFN responsiveness and the sequence diversity of variable region 3 (V3) (aa 2,356–2,379) or surrounding regions near the carboxy terminus of NS5A [Murphy et al., 2002; Sarrazin et al., 2002; Puig-Basagoiti et al., 2005]. A high degree of amino acid substitution in the V3 and pre-V3 regions (aa 2,334–2,355) of NS5A, which is referred to as the IFN/RBV resistance-determining region (IRRDR) (aa 2,334–2,379), has been associated with SVR in Peg-IFN/RBV combination therapy for patients infected with HCV-1b [El-Shamy et al., 2007, 2008]. In addition to these findings in non-structural proteins of the virus, amino acid substitution in a structural region of HCV has been reported to be a predictive viral marker for the virological response to PegIFN/RBV therapy. Amino acid polymorphisms in the HCV core region (Arg70 vs. Gln70 and Leu91 vs. Met91) correlate with virological outcome and on-treatment viral kinetics in Peg-IFN/RBV therapy [Akuta et al., 2006, 2007], and a double wild-type HCV core (Arg70 and Leu91) may be a significant predictor of SVR in Peg-IFN/RBV therapy [Akuta et al., 2007].

Interactions between viral and host proteins in infected cells may influence therapeutic effects and the natural history of infection, since the HCV NS3 region has a significant effect on immunity. The amino-terminal part of this region encodes a serine protease, for which the minimum activity has been mapped to a region between aa 1,059 and 1,204 [Yamada et al., 1998]. The serine protease inactivates Cardif, a caspase recruitment domain (CARD)-containing adaptor protein that interacts with the RNA helicase retinoic acid inducible gene 1 (RIG-1)-dependent antiviral pathway in infected cells [Foy et al., 2003; Meylan et al., 2005; Evans and Seeger, 2006]. This action inhibits phosphorylation and subsequent heterodimerization of interferon regulatory factor-3 (IRF-3), which is essential for activation of IFN signaling through translocation of IRF-3 heterodimers into the nucleus, and eventually blocks IFN-beta production. In addition, inactivation of IRF-3 is postulated to influence the therapeutic effect of IFN-based antiviral therapy, because the IRF-3 heterodimer translocates into the nucleus to bind to the IFN-stimulated response element that produces many antiviral proteins, including 2′,5′-oligoadenylate synthetase and PKR [Nakaya et al., 2001; Grandvaux et al., 2002]. Collectively, these findings suggest that polymorphisms in HCV NS3 structure deduced from sequence variation may influence IFN-related signaling and the antiviral effect of IFN-based anti-HCV therapy.

We have focused on polymorphisms in the secondary structure of the viral polyprotein that interacts with host proteins involved in immunity, with the aim of identification of predictive viral markers for the response to Peg-IFN/RBV therapy. In this study, we examined the potential correlation between polymorphisms in the secondary structure of the HCV NS3 amino-terminal region and virological responses to Peg-IFN/RBV therapy in patients infected with HCV-1b with a high viral load.

PATIENTS AND METHODS

Patients and Treatment Regimen With Peg-IFN Plus Ribavirin

A total of 139 consecutive patients diagnosed with chronic hepatitis C were enrolled in the study from December 2004 to March 2007. These patients included 81 men and 58 women, and were aged from 31 to 75 years old (mean ± SD, 56.8 ± 8.7 years old). All patients were infected with HCV-1b with a high viral load of over 100 KIU/ml, and all received Peg-IFN/RBV therapy. Patients with alcoholic liver injury, autoimmune liver disease, and those who had symptoms of decompensated cirrhosis including ascites were excluded. Briefly, all patients were treated with a combination of Peg-IFN-alpha 2b (Pegintron®; Schering-Plough, Kenilworth, NJ) and RBV (Rebetol®; Schering-Plough) for 48 weeks. Peg-IFN was administered subcutaneously once a week and RBV was given orally twice a day for the total dose. The dosages were determined on the basis of body weight according to the Japanese standard prescription information supplied by the Japanese Ministry of Health, Labour and Welfare, and there was a limit for calculating the optimized dose: patients with body weights of 35–45, 46–60, 61–75, and 76–90 kg were given Peg-IFN at doses of 60, 80, 100, and 120 μg, respectively, and those with body weights of <60, 60–80, and >80 kg were given RBV at doses of 600, 800, and 1,000 mg, respectively. The dose of Peg-IFN or RBV was reduced according to the Japanese standard criteria based on the white blood cell count, neutrophil count, hemoglobin concentration and platelet count [Hiramatsu et al., 2008].

Virological Tests and Response to Peg-IFN Plus Ribavirin

Virological responses were evaluated at 12 weeks after the start of treatment with an early depletion of viremia referred to as an early virological response (EVR), at the end of treatment with depletion of viremia referred to as an end of treatment virological response (ETR), and at 24 weeks after completion of treatment,

with a clinical outcome of a sustained virological response (SVR) representing successful HCV eradication. All patients were negative for hepatitis B surface antigen. Quantification of serum HCV RNA was performed using an RT-PCR-based commercial kit (Amplicor HCV monitor test, ver. 2.0, Roche Diagnostics, Tokyo, Japan). This Amplicor HCV RNA assay has a lower limit of detection of 50 IU/ml. SVR was determined by monitering negativity for HCV RNA monthly for 6 months. The real-time PCR assay kit (COBAS TaqMan HCV Auto, Roche Diagnostics) for more precise quantitation of HCV viremia has recently become available and pre-treatment viral titers were re-evaluated using preserved serum samples. This real-time PCR assay has a lower limit of detection of 15 IU/ml. The study protocol was approved by the Ethics Committee of Yamagata University Hospital. Informed consent was obtained from all patients.

PCR Amplification of the Amino-Terminal Region of NS3

RNA was extracted from 50 µl of serum using an RNeasy Mini kit (Qiagen, Tokyo, Japan). To amplify the region of the HCV genome encoding the amino-terminal region of NS3 (1,027–1,206), a one-step PCR was performed in a tube using the Superscript One-Step RT-PCR kit with Platinum Taq (Gibco-BRL, Tokyo, Japan) and an outer set of primers: NS3-F1 (sense primer; 5′-ACA CCG CGG CGT GTG GGG ACA T-3′; nucleotides 3,295–3,316) and NS3-AS2 (antisense primer; 5′-GCT CTT GCC GCT GCC AGT GGG A-3′; nucleotides 4,040–4,019), as reported previously [Ogata et al., 2002a, 2003]. PCR was initially performed at 45°C for 30 min at RT and then at 94°C for 2 min, followed by the first-round PCR for forty 3-min cycles at 94°, 55°, and 72°C for 1 min each. The second-round PCR was performed with *Pfu* DNA polymerase (Promega, Tokyo, Japan) and an inner set of primers: NS3-F3 (sense primer; 5′-CAG GGG TGG CGG CTC CTT-3′; nucleotides 3,390–3,407) and NS3-AS1 (antisense primer; 5′-GCC ACT TGG AAT GTT TGC GGT A-3′; nucleotides 4,006–3,985). The second-round PCR was performed for 35 cycles, with each cycle consisting of 1 min at 94°C, 1.5 min at 55°C, and 3 min at 72°C. This method allowed amplification of the corresponding portion of the HCV genome from HCV-1b RNA-positive samples. The amplified fragments were purified with a QIAquick PCR purification kit (Qiagen) and directly sequenced (without being subcloned) in both directions using a dRhodamine Terminator Cycle Sequencing Ready Reaction kit and an ABI 377 sequencer (Applied Biosystems, Tokyo, Japan).

Classification of the Secondary Structure of the HCV-1b NS3 Amino-Terminal Region

The secondary structure of the amino-terminal region of HCV NS3 was predicted by computer-assisted Robson analysis [Garnier et al., 1978] with Genetyx-Mac software (ver.10.1; Software Development Co., Tokyo, Japan). Previously, the full-length secondary structure of the HCV-1b NS3 region was analyzed, and this showed that the secondary structure deduced from the carboxy-terminal 60 residues was well conserved in terms of linear structure, without any turn structure [Ogata et al., 2002a]. We have shown that the secondary structure of the 120 residues in the amino-terminal region of HCV-1b NS3 can be classified into two major groups: A and B (Fig. 1) [Ogata et al., 2002a, 2003]. Briefly, the criteria for this classification are as follows: in group A isolates, the carboxy-terminal 20 residues (aa 1,125–1,146) are oriented leftward relative to a domain composed of the remaining amino-terminal region; whereas in group B isolates, the same 20 residues are oriented rightward relative to the rest of the amino-terminal domain.

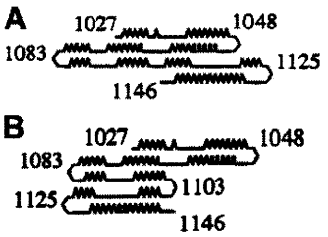

Fig. 1. Secondary structure of the 120 amino-terminal residues of HCV-1b nonstructural 3 (NS3) region classified into two major groups: A and B. The looped, zigzag, straight, and bent lines represent α-helix, β-sheet, coil, and turn structures, respectively. The numbers indicate amino acid positions. **A**: Group A, (**B**) Group B.

Analysis of Amino Acid Substitutions in the Core Region

To amplify a region of the HCV genome encoding the core region including positions 70 and 91, reverse transcription and the first-round PCR were performed in a tube by the Superscript One-Step RT-PCR kit with Platinum *Taq* (Gibco-BRL) and an outer set of primers, followed by second-round PCR with an inner set of primers in accordance with procedures reported previously [Ogata et al., 2002b]. The sequences of the amplified fragments were determined by direct sequencing.

Statistical Analysis

Data were analyzed by a χ^2 test for independence with a two-by-two contingency table and a Student *t*-test. A *P*-value <0.05 was considered significant.

RESULTS

Virological Response *and Adherence* to the Peg-IFN Plus Ribavirin Regimen

Rates of virological responses in patients treated with PegIFN/RBV combination therapy for 48 weeks are shown in Figure 2. Of the 139 patients enrolled in the study, SVR, non-SVR and cessation of therapy occurred in 58 (42%), 62 (45%), and 19 (14%), respectively. Serious

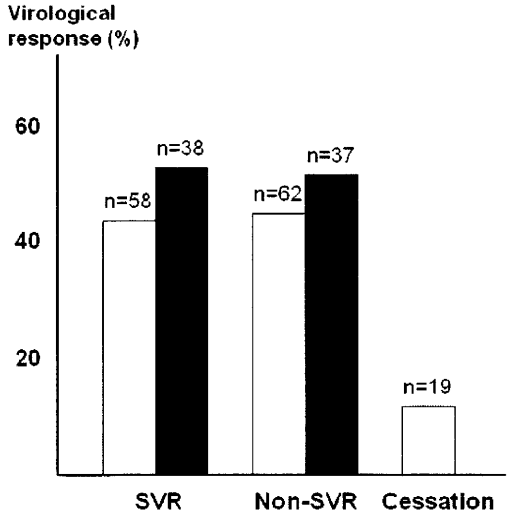

Fig. 2. Virological response in patients treated with peginterferon plus ribavirin for 48 weeks. The results are shown for all 139 subjects (open bars) and for 75 cases with good adherence of >80% of the scheduled dosages (closed bars). SVR, sustained virological response.

adverse events that necessitated discontinuation of this therapy were depression in one patient, thyroid function disorder in 2, general itching in 2, infection in 2, anorexia in 2, occurrence of hepatocellular carcinoma in 2, and a decreased neutrophil count in 2. Six patients also terminated this therapy at their own request. Of the 139 patients, 75 (54%) received >80% of the scheduled dosage of Peg-IFN and RBV designated before treatment, and of these 75 cases SVR and non-SVR occurred in 38 (51%) and 37 (49%), respectively.

Prevalence of Types of Secondary Structure of the Amino-Terminal Region of HCV NS3

The prevalence of the types of secondary structure of HCV NS3 in the 139 subjects is shown in Table I. Among these subjects, 43 (31%), 70 (50%), and 26 (19%) were classified into groups A, B, and others, including 3 of mixed type (A plus B) and 23 of non-A, non-B type. Of the 75 cases with good adherence to administration of >80% of the scheduled dosage, 28 (37%), 40 (53%) and 7 (9%) were classified into groups A, B, and others. The amino acid data of group A and B in the cases with good adherence to administration are available in the DDBJ/EMBL/GenBank databases with the accession numbers AB548070–AB548137. Our analysis revealed no specific correlations between amino acid sequences and the secondary structure deduced by the Robson method, as we have reported previously [Ogata et al., 2003].

TABLE I. Prevalence of the HCV NS3 Secondary Structure Type

	Group A (%)	Group B (%)	Others (%)
Enrolled cases (n = 139)	43 (31)	70 (50)	26 (19)
Adherent cases (n = 75)	28 (37)	40 (53)	7 (9)

Characteristics of Adherent Patients Based on Different HCV NS3 Structure Types

The virological responses to Peg-IFN/RBV combination therapy for patients infected with group A and B isolates were assessed in the 68 subjects with good adherence to the scheduled dosage of Peg-IFN and RBV. The characteristics of patients infected with group A and B isolates are shown in Table II. Age, gender, pre-treatment level of serum HCV RNA and ALT, and frequency of fibrosis stage did not differ significantly between the two groups. Peg-IFN/RBV combination therapy was completed in all the patients, and the total administered dosages of Peg-IFN and RBV was >95% of the scheduled dosage in both groups.

Relationship Between Virological Responses and Polymorphisms in the HCV NS3 Amino-Terminal Region

In the 68 patients who received >95% of the scheduled doses of Peg-IFN and RBV for 48 weeks, SVR and non-SVR occurred in 33 (49%) and 35 (51%), respectively. The EVR, ETR, and SVR rates in patients infected with group A and B isolates are shown in Table III. There was a significant difference in the rates of EVR between subjects infected with group A and B isolates: EVR was achieved in 19 of 28 (68%) patients with group A infection, compared to 17 of 40 (43%) with group B infection ($P < 0.05$). The final outcome also differed significantly between subjects infected with group A and B isolates: SVR was achieved in 18 of 28 (64%) patients with group A infection, compared to 15 of 40 (38%) with group B infection ($P < 0.05$).

Polymorphisms in Core Amino Acids 70/91 and in the HCV NS3 Secondary Structure

The wild-type core sequence (Arg70, Leu91) has been associated with SVR in Peg-IFN/RBV combination therapy, while the non-double wild-type containing one or two substitutions at positions 70 and/or 91 was associated with non-SVR [Akuta et al., 2007]. Therefore, we examined substitutions at positions 70 and 91 in the HCV core region in pre-treatment serum samples of 44 cases that were available for testing. The double wild-type 70/91 sequence was found in 22 of the 44 cases (50%), of which 12 were SVR and 10 were non-SVR. Combination analysis of polymorphisms of the HCV core 70/91 positions and the NS3 amino-terminal region showed that 10 (83%) of the 12 SVR cases and only 3 (30%) of the 10 non-SVR cases with the double wild-type core had a group A polymorphism in HCV NS3 (Table IV). Thus, combination analysis of the core and NS3 regions may improve prediction of the outcome of Peg-IFN/RBV therapy.

TABLE II. Characteristics of Adherent Patients Infected With HCV Group A and B Isolates

	Group A (n = 28)	Group B (n = 40)	P
Age (years)	55.5 ± 9.5	55.5 ± 8.9	NS[a]
Sex (men/women)	18/10	21/19	NS[b]
Pre-treatment HCV RNA (KIU/ml)	1,635 ± 930	2,087 ± 1,422	NS[a]
Alanine aminotransferase level (U/L)	80 ± 62	71 ± 47	NS[a]
Stage of liver fibrosis			
F1 or F2/F3 or F4	19/9	28/12	NS[b]
Drug adherence dosage (%)			
Pegylated interferon	97.7 ± 5.2	95.2 ± 7.3	NS[a]
Ribavirin	96.8 ± 6.4	95.3 ± 7.7	NS[a]

NS, not significant.
[a] t-test.
[b] χ^2 test.

Re-Evaluation of Pre-Treatment HCV Viremia Status Using Real-Time PCR

Since the viral titer before treatment is a major predictive marker of the outcome of Peg-IFN/RBV therapy, we re-evaluated the pre-treatment viral titers more precisely using preserved serum samples taken within 1 month before treatment, using a real-time PCR assay. The pre-treatment viral titers did not differ significantly between sera with group A and B isolates (5.98 ± 0.94 vs. 6.25 ± 0.62 logIU/ml) (Table V). The secondary structure polymorphisms of HCV NS3 were independent of the pre-treatment viral titers.

DISCUSSION

Antiviral therapy with Peg-IFN/RBV for 48 weeks fails to eradicate HCV in about half of patients infected with a high titer of HCV genotype 1b, and the severe adverse events and high costs associated with this therapy require outcome prediction to allow targeted treatment for chronic hepatitis C. The pre-treatment viral titer, viral factors that influence the virological response to IFN-based anti-HCV therapy have been widely investigated. Viral kinetics showing prompt seronegativity after the start of treatment is a critical factor for achieving SVR, and thus the possible correlation between an early virological response and genetic sequence variation of the HCV has been studied. In particular, amino acid substitutions in the HCV core region at positions 70 and 91 or multiple mutations detected in the IRRDR of the HCV NS5A region are useful markers for predicting EVR and subsequent SVR.

TABLE III. Virological Responses in Subjects With Different Polymorphisms in the Secondary Structure of HCV NS3

	EVR*	ETR**	SVR*
Group A (n = 28)	19 (68%)	23 (82%)	18 (64%)
Group B (n = 40)	17 (43%)	25 (63%)	15 (38%)

EVR: early virological response at 12 weeks after the start of treatment.
ETR: virological response at the end of treatment.
SVR: sustained virological response 24 weeks after completion of treatment.
*$P < 0.05$.
**$P = 0.08$; χ^2 test.

To date, the influence of several single amino acid substitutions and accumulation of these changes in the viral genome on the effect of IFN-based anti-HCV therapy has been examined. Since interactions between host and viral proteins in infected cells may influence the therapeutic effect of an antiviral agent, we focused on the association of structural polymorphism of a viral protein with the effect of Peg-IFN/RBV combination therapy in this study. Our results suggest that polymorphism analysis of secondary structure deduced from sequence variations in the HCV NS3 amino-terminal region can be used to predict viral responses to this therapy.

Amino acid sequences of the HCV NS3 amino-terminal region, which encodes a serine protease, vary greatly among HCV isolates. Interactions between HCV NS3 and host proteins may influence both oncogenesis and immunity, and thus elucidation of the biological significance of these interactions could result in a new prognostic marker for HCC or a predictive marker for anti-HCV therapy. First, HCV NS3 interacts with the p53 tumor suppressor to suppress p53-dependent apoptosis or p21 transcriptional activity [Ishido and Hotta, 1998; Kwun et al., 2001; Deng et al., 2006]. Transfection of a plasmid expressing the amino-terminal portion of HCV NS3 induces cell transformation in vitro, and transplanted cells proliferate with sarcoma-like features in vivo [Sakamuro et al., 1995]. These findings suggest that NS3 may be involved in the oncogenic pathway in HCV infection. We have shown that the secondary structure of the 120-residue amino-terminal region of NS3 (1,027–1,146) is classifiable into two major groups: A and B. This region encodes a serine protease and also includes p53-binding sites. Our

TABLE IV. Treatment Outcome of Cases With a Double Wild-Type Core Region and Different HCV NS3 Structural Polymorphism

	Group A (%)	Group B (%)	P
SVR (n = 12)	10 (83)	2 (17)	0.02[a]
Non-SVR (n = 10)	3 (30)	7 (70)	

SVR, sustained virological response.
[a] χ^2 test.

TABLE V. Pre-Treatment HCV RNA Levels Measured by Real-Time PCR for Subjects With Different HCV NS3 Structural Polymorphism

	Group A	Group B	*P*
SVR (n = 33)	5.78 ± 1.05	6.13 ± 0.71	NS[a]
Non-SVR (n = 35)	6.33 ± 0.59	6.32 ± 0.55	NS[a]
Total (n = 68)	5.98 ± 0.94	6.25 ± 0.62	NS[a]

SVR, sustained virological response. NS, not significant.
[a]*t* test.

previous cross-sectional studies revealed that the prevalence of group B infection is significantly higher in HCC cases than in non-HCC cases [Ogata et al., 2003], and that the group B infection is an independent risk factor for development of HCC in patients with chronic HCV infection [Nishise et al., 2007]. Second, NS3 interacts with host proteins associated with IFN signaling and thus influences cellular immunity. Since the serine protease encoded by the amino-terminal region of NS3 inhibits the IFN-signaling pathway, polymorphism of this region is likely to influence the effect of Peg-IFN/RBV combination therapy.

Several factors associated with the virological response to this therapy are well known, with adherence to both IFN and RBV strongly influencing outcome [Pearlman, 2004; Arase et al., 2005; Yamada et al., 2008]. In this study, we analyzed 75 cases in which >80% of the scheduled dosage of both drugs was administered. Of these cases, 28 (37%) and 40 (53%) were infected with group A and B isolates, respectively, which were similar rates to those for the 139 cases in the overall study. Age, gender, viral load before treatment, ALT level, proportion of fibrosis stage and adherence to Peg-IFN and RBV did not differ between the group A and B cases. However, the frequencies of SVR and EVR were significantly higher in group A, and those for non-EVR and non-SVR were significantly higher in group B. The results suggest that infection with the group B isolate, which correlates with a higher rate of HCC, is resistant to Peg-IFN/RBV therapy. The pre-treatment viremia status in the 68 cases with group A or B isolates showed no significant differences between the two groups of patients. Therefore, these results suggest that the secondary structure of the HCV NS3 amino-terminal region may be useful for prediction of the outcome of Peg-IFN/RBV combination therapy. In this initial study setting, the relationship of these polymorphisms to the frequency of rapid viral response at 4 weeks after the start of treatment was not evaluated. It will be important to assess this relationship in a future study.

The polymorphism in HCV core region (Arg70/Leu91) is a useful predictive marker for virological responses in Peg-IFN/RBV therapy [Akuta et al., 2007]. Interestingly, a combined analysis of polymorphisms of the core region (which encodes a structural protein) and HCV NS3 (a nonstructural protein) improved the prediction rate. Therefore, analysis of NS3 polymorphism in combination with the core structural polymorphism appears to improve prediction of the outcome of Peg-IFN/RBV therapy. A larger, multi-center prospective study would be necessary to validate the present results. In conclusion, the results of this study suggest that secondary structure polymorphism in the amino-terminal region of HCV NS3 is a useful predictive marker of the effect of Peg-IFN/RBV combination therapy for chronic hepatitis C. Although the present findings are clinically important, and will be helpful for predicting the outcome of Peg-IFN/RBV therapy, further in vitro studies will be needed to elucidate the molecular mechanism underlying the association of HCV NS3polymorphisms with clinical outcome.

REFERENCES

Akuta N, Suzuki F, Sezaki H, Suzuki Y, Hosaka T, Someya T, Kobayashi M, Saitoh S, Watahiki S, Sato J, Kobayashi M, Arase Y, Ikeda K, Kumada H. 2006. Predictive factors of virological non-response to interferon-ribavirin combination therapy for patients infected with hepatitis C virus of genotype 1b and high viral load. J Med Virol 78:83–90.

Akuta N, Suzuki F, Kawamura Y, Yatsuji H, Sezaki H, Suzuki Y, Hosaka T, Kobayashi M, Kobayashi M, Arase Y, Ikeda K, Kumada H. 2007. Predictive factors of early and sustained responses to peginterferon plus ribavirin combination therapy in Japanese patients infected with hepatitis C virus genotype 1b: Amino acid substitutions in the core region and low-density lipoprotein cholesterol levels. J Hepatol 46:403–410.

Arase Y, Ikeda K, Tsubota A, Suzuki F, Suzuki Y, Saitoh S, Kobayashi M, Akuta N, Someya T, Hosaka T, Sezaki H, Kobayashi M, Kumada H. 2005. Significance of serum ribavirin concentration in combination therapy of interferon and ribavirin for chronic hepatitis C. Intervirology 48:138–144.

Bruno S, Cammà C, Di Marco V, Rumi M, Vinci M, Camozzi M, Rebucci C, Di Bona D, Colombo M, Craxì A, Mondelli MU, Pinzello G. 2004. Peginterferon alfa-2b plus ribavirin for naïve patients with genotype 1 chronic hepatitis C: A randomized controlled trial. J Hepatol 41:474–481.

Deng L, Nagano-Fujii M, Tanaka M, Nomura-Takigawa Y, Ikeda M, Kato N, Sada K, Hotta H. 2006. NS3 protein of hepatitis C virus associated with the tumor suppressor p53 and inhibits its function in an NS3 sequence-dependent manner. J Gen Virol 87:1703–1713.

El-Shamy A, Sasayama M, Nagano-Fujii M, Sasase N, Imoto S, Kim SR, Hotta H. 2007. Prediction of efficient virological response to pegylated interferon/ribavirin combination therapy by NS5A sequences of hepatitis C virus and anti-NS5A antibodies in pre-treatment sera. Microbiol Immunol 51:471–482.

El-Shamy A, Nagano-Fujii M, Sasase N, Imoto S, Kim SR, Hotta H. 2008. Sequence variation in hepatitis C virus nonstructural protein 5A predicts clinical outcome of pegylated interferon/ribavirin combination therapy. Hepatology 48:38–47.

Enomoto N, Sakuma I, Asahina Y, Kurosaki M, Murakami T, Yamamoto C, Ogura Y, Izumi N, Marumo F, Sato C. 1996. Mutations in the nonstructural protein 5A gene and response to interferon in patients with chronic hepatitis C virus 1b infection. N Engl J Med 334:77–81.

Evans JD, Seeger C. 2006. Cardif: A protein central to innate immunity is inactivated by the HCV NS3 serine protease. Hepatology 43:615–617.

Foy E, Li K, Wang C, Sumpter R, Jr., Ikeda M, Lemon SM, Gale M, Jr. 2003. Regulation of interferon regulatory factor-3 by the hepatitis C virus serine protease. Science 300:1145–1148.

Gale MJ, Jr., Korth MJ, Tang NM, Tan SL, Hopkins DA, Dever TE, Polyak SJ, Gretch DR, Katze MG. 1997. Evidence that hepatitis C virus resistance to interferon is mediated through repression of the PKR protein kinase by the nonstructural 5A protein. Virology 230:217–227.

Gale MJ, Jr., Korth MJ, Katze MG. 1998. Repression of the PKR protein kinase by the hepatitis C virus NS5A protein: A potential mechanism of interferon resistance. Clin Diagn Virol 10:157–162.

Garnier J, Osguthorfe DJ, Robson B. 1978. Analysis of the accuracy and implications of simple methods for predicting the secondary structure of globular proteins. J Mol Biol 120:97–120.

Grandvaux N, Servant MJ, tenOever B, Sen GC, Balachandran S, Barber GN, Lin R, Hiscott J. 2002. Transcriptional profiling of interferon regulatory factor 3 target genes: Direct involvement in the regulation of interferon-stimulated genes. J Virol 76:5532–5539.

Hadziyannis SJ, Sette H, Jr., Morgan TR, Balan V, Diago M, Marcellin P, Ramadori G, Bodenheimer H, Jr., Bernstein D, Rizzetto M, Zeuzem S, Pockros PJ, Lin A, Ackrill AM. 2004. Peginterferon-alpha2a and ribavirin combination therapy in chronic hepatitis C: A randomized study of treatment duration and ribavirin dose. Ann Intern Med 140:346–355.

Hiramatsu N, Kurashige N, Oze T, Takehara T, Tamura S, Kasahara A, Oshita M, Katayama K, Yoshihara H, Imai Y, Kato M, Kawata S, Tsubouchi H, Kumada H, Okanoue T, Kakumu S, Hayashi N. 2008. Early decline of hemoglobin can predict progression of hemolytic anemia during pegylated interferon and ribavirin combination therapy in patients with chronic hepatitis C. Hepatol Res 38:52–59.

Ishido S, Hotta H. 1998. Complex formation of the nonstructural protein 3 of hepatitis C virus with the p53 tumor suppressor. FEBS Lett 438:258–262.

Kwun HJ, Jung EY, Ahn JY, Lee MN, Jang KL. 2001. p53-dependent transcriptional repression of p21(waf1) by hepatitis C virus NS3. J Gen Virol 82:2235–2241.

Manns MP, McHutchison JG, Gordon SC, Rustgi VK, Shiffman M, Reindollar R, Goodman ZD, Koury K, Ling M, Albrecht JK. 2001. Peginterferon alfa-2b plus ribavirin compared with interferon alfa-2b plus ribavirin for initial treatment of chronic hepatitis C: A randomized trial. Lancet 358:958–965.

Meylan E, Curran J, Hofmann K, Moradpour D, Binder M, Bartenschlager R, Tschopp J. 2005. Cardif is an adaptor protein in the RIG-I antiviral pathway and is targeted by hepatitis C virus. Nature 437:1167–1172.

Murphy MD, Rosen HR, Marousek GI, Chou S. 2002. Analysis of sequence configurations of the ISDR, PKR-binding domain, and V3 region as predictors of response to induction interferon-alpha and ribavirin therapy in chronic hepatitis C infection. Dig Dis Sci 47:1195–1205.

Nakaya T, Sato M, Hata N, Asagiri M, Suemori H, Noguchi S, Tanaka N, Taniguchi T. 2001. Gene induction pathways mediated by distinct IRFs during viral infection. Biochem Biophys Res Commun 283:1150–1156.

Nishise Y, Saito T, Sugahara K, Ito JI, Saito K, Togashi H, Nagano-Fujii M, Hotta H, Kawata S. 2007. Risk of hepatocellular carcinoma and secondary structure of hepatitis C virus (HCV) NS3 protein amino-terminus, in patients infected with HCV subtype 1b. J Infect Dis 196:1006–1009.

Nousbaum J, Polyak SJ, Ray SC, Sullivan DG, Larson AM, Carithers RL, Jr., Gretch DR. 2000. Prospective characterization of full-length hepatitis C virus NS5A quasispecies during induction and combination antiviral therapy. J Virol 74:9028–9038.

Ogata S, Ku Y, Yoon S, Makino S, Nagano-Fujii M, Hotta H. 2002a. Correlation between secondary structure of an amino-terminal portion of the nonstructural protein 3 (NS3) of hepatitis C virus and development of hepatocellular carcinoma. Microbiol Immunol 46:549–554.

Ogata S, Nagano-Fujii M, Ku Y, Yoon S, Hotta H. 2002b. Comparative sequence analysis of the core protein and its frameshift product, the F protein, of hepatitis C virus subtype 1b strains obtained from patients with and without hepatocellular carcinoma. J Clin Microbiol 40:3625–3630.

Ogata S, Florese RH, Nagano-Fujii M, Hidajat R, Deng L, Ku Y, Yoon S, Saito T, Kawata S, Hotta H. 2003. Identification of hepatitis C virus (HCV) subtype 1b strains that are highly, or only weakly, associated with hepatocellular carcinoma on the basis of the secondary structure of an amino-terminal portion of the HCV NS3 protein. J Clin Microbiol 41:2835–2841.

Pearlman BL. 2004. Hepatitis C treatment update. Am J Med 117:344–352.

Puig-Basagoiti F, Forns X, Furcić I, Ampurdanés S, Giménez-Barcons M, Franco S, Sánchez-Tapias JM, Saiz JC. 2005. Dynamics of hepatitis C virus NS5A quasispecies during interferon and ribavirin therapy in responder and non-responder patients with genotype 1b chronic hepatitis C. J Gen Virol 86:1067–1075.

Sakamuro D, Furukawa T, Takegami T. 1995. Hepatitis C virus nonstructural protein NS3 transforms NIH 3T3 cells. J Virol 69: 3893–3896.

Sarrazin C, Herrmann E, Bruch K, Zeuzem S. 2002. Hepatitis C virus nonstructural 5A protein and interferon resistance: A new model for testing the reliability of mutational analyses. J Virol 76:11079–11090.

Yamada K, Mori A, Seki M, Kimura J, Yuasa S, Matsuura Y, Miyamura T. 1998. Critical point mutations for hepatitis C virus NS3 proteinase. Virology 246:104–112.

Yamada G, Iino S, Okuno T, Omata M, Kiyosawa K, Kumada H, Hayashi N, Sakai T. 2008. Virological response in patients with hepatitis C virus genotype 1b and a high viral load: Impact of peginterferon-alpha-2a plus ribavirin dose reductions and host-related factors. Clin Drug Investig 28:9–16.

Original Paper

Intervirology

Intervirology
DOI: 10.1159/000322219

Received: May 12, 2010
Accepted after revision: October 14, 2010
Published online: February 4, 2011

Polymorphisms of Hepatitis C Virus Non-Structural Protein 5A and Core Protein and Clinical Outcome of Pegylated-Interferon/Ribavirin Combination Therapy

Ahmed El-Shamy[a, c] Soo-Ryang Kim[b] Yoshi-Hiro Ide[a] Noriko Sasase[b]
Susumu Imoto[b] Lin Deng[a] Ikuo Shoji[a] Hak Hotta[a]

[a]Division of Microbiology, Center for Infectious Diseases, Kobe University Graduate School of Medicine, and [b]Division of Gastroenterology, Kobe Asahi Hospital, Kobe, Japan; [c]Department of Virology, Suez Canal University Faculty of Veterinary Medicine, Ismalia, Egypt

Key Words
Hepatitis C virus · Non-structural protein 5A · Interferon/ribavirin resistance-determining region · Interferon sensitivity-determining region · Core protein · Sustained virological response · Prediction

Abstract
Objective: Hepatitis C virus (HCV genome) polymorphisms are thought to influence the outcome of pegylated-interferon/ribavirin (PEG-IFN/RBV) therapy. This study aimed to examine non-structural protein 5A (NS5A) polymorphisms, e.g. IFN/RBV resistance-determining region (IRRDR) and IFN sensitivity-determining region (ISDR), and core protein polymorphism as predictive therapeutic markers. ***Methods:*** Pretreatment sequences of NS5A and core regions were analyzed in 68 HCV-1b-infected patients treated with PEG-IFN/RBV. ***Results:*** Of 24 patients infected with HCV having an IRRDR with 6 or more mutations (IRRDR≥6), 18 (75%) patients achieved sustained virological response (SVR), whereas only 11 (25%) of 44 patients infected with HCV having IRRDR≤5 did. IRRDR≥6 was significantly associated with SVR ($p < 0.0001$). On the other hand, ISDR≥2 was significantly associated with relapse (either before [breakthrough] or after end-of-treatment response [ETR-relapse]) ($p < 0.05$) and a point mutation of the core protein from Arg to Gln at position 70 (Gln^{70}) was significantly associated with null-response ($p < 0.05$). Multivariate analysis identified IRRDR≥6 as the only viral genetic factor that independently predicted SVR. ***Conclusion:*** NS5A (IRRDR and ISDR) and core protein polymorphisms are associated with the outcome of PEG-IFN/RBV therapy for chronic hepatitis C. In particular, IRRDR≥6 is a useful marker for prediction of SVR.

Introduction

Hepatitis C virus (HCV) is the major cause of chronic liver diseases worldwide [1]. As a consequence of the long-term persistence of chronic hepatitis C, the number of patients with hepatocellular carcinoma is expected to increase further over the next 20 years [2]. To reduce the impact of this worldwide health problem, efficient treatment is required. Currently, a combination therapy of pegylated-interferon-α and ribavirin (PEG-IFN/RBV) is a

KARGER
Fax +41 61 306 12 34
E-Mail karger@karger.ch
www.karger.com

0300–5526/11/0000–0000$38.00/0

Accessible online at:
www.karger.com/int

Hak Hotta, MD, PhD
Division of Microbiology, Center for Infectious Diseases
Kobe University Graduate School of Medicine
7-5-1 Kusunoki-cho, Chuo-ku, Kobe 650-0017 (Japan)
Tel. +81 78 382 5500, Fax +81 78 382 5519, E-Mail hotta@kobe-u.ac.jp

standard treatment for chronic hepatitis C [3]. However, this therapy is sometimes difficult to tolerate and results in a sustained virological response (SVR) in only ~50% of patients, especially those infected with the most resistant genotypes, HCV-1a and HCV-1b [3]. Given the considerable side effects, the possibility of discontinuation and the high cost of this treatment, prediction of treatment outcome is needed. An expanded range of predictors may assist clinicians and patients in more accurately assessing the likelihood of an SVR and thus in making more informed treatment decisions [4].

Since the HCV genotype is one of the major factors affecting the IFN-based therapy response, IFN resistance is, at least partly, genetically encoded by HCV itself [5]. In this context, non-structural protein 5A (NS5A) has been widely discussed for its correlation with IFN responsiveness. Enomoto et al. [6] proposed that sequence variations within a region in NS5A spanning from amino acids (aa) 2,209 to 2,248, called the IFN sensitivity-determining region (ISDR), is correlated with IFN responsiveness. Recently, we identified a new region near the C-terminus of NS5A spanning from aa 2,334 to 2,379, which we referred to as the IFN/RBV resistance-determining region (IRRDR) [7]. The degree of sequence variation within IRRDR was significantly associated with the clinical outcome of PEG-IFN/RBV combination therapy. On the other hand, prediction of SVR by aa substitutions within the core protein in Japanese patients infected with HCV-1b has also been proposed [8, 9]. In multivariate analysis, the criterion of double-wild core, presence of Arg at position 70 and Leu at position 91 (Arg^{70}/Leu^{91}), was identified as an independent SVR predictor.

This study aimed to examine NS5A polymorphisms, including those in IRRDR and ISDR, and core polymorphism as predictive markers for HCV treatment outcome. The core protein with Arg^{70}/Leu^{91} was defined as wild-core while the other patterns as non-wild-core. The possible correlation of either Arg^{70} alone or Leu^{91} alone with the clinical outcome of PEG-IFN/RBV therapy was also examined.

Patients and Methods

Patients

A total of 68 patients seen at Kobe Asahi Hospital in Kobe, Japan, who were chronically infected with HCV-1b, with diagnoses based on anti-HCV antibody detection and HCV-RNA detection, were enrolled in the study. HCV subtype was determined as according to the method of Okamoto et al. [10]. Patients were treated with PEG-IFNα-2b (Pegintron®; Schering-Plough, Kenilworth, N.J., USA) (1.5 μg/kg b.w., once weekly, s.c.) and RBV (Rebetol®; Schering-Plough) (600–800 mg daily, per os), according to a standard treatment protocol for Japanese patients established by a hepatitis study group of the Ministry of Health, Labor and Welfare, Japan. All patients received >80% of scheduled dosage of PEG-IFN and RBV. Serum samples were collected from the patients at intervals of 4 weeks before, during and after the treatment, and tested for HCV RNA and core antigen titers as reported previously [11].

The study protocol was approved beforehand by the Ethic Committee in Kobe Asahi Hospital, and written informed consent was obtained from each patient prior to the treatment.

Sequence Analysis of HCV NS5A and Core

HCV RNA was extracted from 140 μl of serum using a commercially available kit (QIAmp viral RNA kit; Qiagen, Tokyo, Japan). Amplification of full-length NS5A and core regions of the HCV genome were performed as described elsewhere [7, 11, 12]. The sequences of the amplified fragments of NS5A and core regions were determined by direct sequencing. The aa sequences were deduced and aligned using Genetyx Win software version 7.0 (Genetyx Corp., Tokyo, Japan).

Statistical Analysis

Statistical differences in the patients' baseline parameters according to the degree of IRRDR polymorphism were determined by Student's t test for numerical variables and Fisher's exact probability test for categorical variables. Likewise, statistical differences in treatment responses according to NS5A and core polymorphisms were determined by Fisher's exact probability test. Kaplan-Meier HCV survival curve analysis was performed based on serum HCV-RNA positivity data during the treatment period (48 weeks) according to NS5A and core polymorphisms. The data obtained were evaluated by the log-rank test. Uni- and multivariate logistic analyses were performed to identify variables that independently predicted the treatment outcome. Variables with a p value of <0.1 in univariate analysis were included in a multivariate logistic regression analysis. The odds ratios and 95% confidence intervals (95% CI) were also calculated. All statistical analyses were performed using SPSS version 16 software (SPSS Inc., Chicago, Ill., USA). Unless otherwise stated, a p value <0.05 was considered as statistically significant.

Nucleotide Sequence Accession Numbers

The sequence data reported in this paper have been deposited in the DDBJ/EMBL/GenBank nucleotide sequence databases under the accession numbers AB285035 through AB285081, AB354116 through AB354118, and AB518774 through AB518861.

Results

Patients' Responses to PEG-IFN/RBV Combination Therapy

Among 68 patients enrolled in this study, HCV-RNA negativity was achieved by 8 (12%) patients at week 4 (rapid virological response [RVR]), 36 (53%) patients at week 12 (early virological response [EVR]), 47 (69%) patients at

Table 1. Proportions of various virological responses of patients treated with PEG-IFN/RBV

Virological response	Proportion, patients	
	n/total	%
RVR	8/68	12
EVR	36/68	53
ETR	47/68	69
SVR	29/68	43
Non-SVR	39/68	57
Null-response	17/68	25
ETR-relapse	18/68	26
Breakthrough	4/68	6

PEG-IFN/RBV = Pegylated-interferon/ribavirin; RVR = rapid virological response; EVR = early virological response; ETR = end-of-treatment response; SVR = sustained virological response.

week 48 (end-of-treatment response [ETR]) and 29 (43%) patients at week 72 (SVR) (table 1). A total of 39 patients (57%) failed to achieve SVR and they were referred to as non-SVR. Non-SVR can be further divided into three categories: (i) null-response, which is defined by continued presence of serum HCV RNA during the entire period of the treatment and follow-up; (ii) breakthrough, defined as transient disappearance of HCV RNA followed by its reappearance before the end of the 48-week treatment, and (iii) ETR-relapse, defined by reappearance of HCV RNA after ETR has been achieved. Seventeen (25%) patients were null-response while 18 (26%) and 4 (6%) patients were ETR-relapse and breakthrough, respectively (table 1).

Correlation between NS5A Polymorphism and Treatment Responses

Using a receiver operating characteristic curve analysis, 6 mutations in IRRDR were previously estimated as an optimal cutoff number of mutations for SVR prediction [7]. Initially the correlation between the patients' demographical, hematological, biochemical and virological baseline parameters and the degree of IRRDR polymorphism was examined. This analysis revealed that patient's sex was the only factor that significantly correlated to the degree of IRRDR polymorphism since 49% (17/35) of males were infected with HCV isolates having IRRDRs with 6 mutations or more (IRRDR≥6) compared to 21% (7/33) of females ($p = 0.02$) (table 2). HCV-RNA titers or HCV core antigen titers did not differ significantly between patients infected with HCV isolates of IRRDR≥6 and those of IRRDR≤5.

Next, the possible correlation between IRRDR polymorphism and the ultimate treatment responses was examined. Among 24 patients infected with HCV isolates of IRRDR≥6, 18 (75%), 6 (25%), 3 (12.5%) and 3 (12.5%) patients were SVR, non-SVR, null-response and relapse (ETR-relapse *plus* breakthrough), respectively (table 3). By contrast, among 44 patients infected with HCV isolates of IRRDR≤5, 11 (25%), 33 (75%), 14 (32%) and 19 (43%) patients were SVR, non-SVR, null-response and relapse (ETR-relapse *plus* breakthrough), respectively. The proportions of different treatment responses among HCV isolates with IRRDR≥6 and IRRDR≤5 were significantly different. Furthermore, patients infected with HCV isolates with Ala at position 2360 (Ala^{2360}) in IRRDR had a more significant likelihood of SVR than those infected with HCV isolates with non-Ala^{2360}, who tended to be non-SVR, in particular null-response (table 3; fig. 1).

As the IRRDR polymorphism was closely correlated with the ultimate treatment responses, it was also significantly correlated with the on-treatment responses, in particular EVR and ETR (table 4). However, there was no significant correlation between the IRRDR polymorphism and RVR. Also, the presence of Ala^{2360} was correlated significantly with ETR.

Regarding the analysis of ISDR polymorphism and its correlation to the treatment responses, first, the criterion of ISDR with 4 mutations or more (ISDR≥4), the initial criterion of IFN responsiveness proposed by Enomoto et al. [6] was tested. Since the prevalence of ISDR≥4 was only 9% (6/68) of all isolates analyzed, this criterion did not significantly correlate with the treatment responses (data not shown). Next, the correlation between the treatment responses and ISDR mutations at a cutoff point of 2 mutations, a newly proposed ISDR criterion of PEG-IFN/RBV responsiveness [13, 14] was tested. Although there was no significant difference in the proportions of SVR and non-SVR between HCV isolates with ISDR of 2 mutations or more (ISDR≥2) and those of ISDR≤1, a small but significant difference in the proportions of SVR and relapse (ETR-relapse *plus* breakthrough) was observed between ISDR≥2 and ISDR≤1 (table 3). Interestingly, ISDR polymorphism was the only virological factor examined in this study that showed a significant correlation with RVR (table 4). However, this correlation disappeared when further time points of treatment course, such as EVR and ETR, were considered.

Table 2. Correlation between IRRDR polymorphism and patients' demographic characteristics

Factor	IRRDR≥6	IRRDR≤5	p value
Age, mean ± SD	58.71 ± 8.44	59.61 ± 10.30	0.71
Sex, male/female	17/7	18/26	0.02
Body weight, kg	59.87 ± 9.56	58.20 ± 11.92	0.56
Platelets, $\times 10^4/mm^3$	17.22 ± 5.5	14.96 ± 4.71	0.16
Hemoglobin, g/dl	14.25 ± 1.48	13.55 ± 1.77	0.11
γ-GTP, IU/l	49.50 ± 44.29	55.60 ± 65.60	0.69
GPT, IU/l	47.54 ± 33.09	49.33 ± 34.78	0.84
HCV-RNA, KIU/ml	2,070.21 ± 1,720.27	2,038.57 ± 1,963.05	0.95
HCV core antigen, fmol/l	6,750.87 ± 6,859.82	9,320.52 ± 10,636.48	0.30

IRRDR = Interferon/ribavirin resistance-determining region; γ-GTP = γ-guanosine triphosphate; GPT = glutamic pyruvate transaminase.

Table 3. Correlation between NS5A and core protein polymorphisms and ultimate virological responses of patients treated with PEG-IFN/RBV

Protein	Factor	Total[a]	SVR[b]	Non-SVR	Null-response	Relapse (ETR-relapse *plus* breakthrough)	p value		
							SVR vs. non-SVR	SVR vs. null-response	SVR vs. relapse (ETR-relapse *plus* breakthrough)
NS5A	IRRDR≥6	24	18 (75)[c]	6 (25)	3 (12.5)	3 (12.5)	<0.0001	0.005	0.0006
	IRRDR≤5	44	11 (25)	33 (75)	14 (32)	19 (43)			
	Ala^{2360}	18	12 (67)	6 (33)	1 (5)	5 (28)	0.026	0.016	0.2
	Non-Ala^{2360}	50	17 (34)	33 (66)	16 (32)	17 (34)			
	ISDR≥2	18	10 (56)	8 (44)	6 (33)	2 (11)	0.27	1.0	0.048
	ISDR≤1	50	19 (38)	31 (62)	11 (22)	20 (40)			
Core	Wild-core (Arg^{70}/Leu^{91})	33	18 (55)	15 (45)	5 (15)	10 (30)	0.1	0.07	0.27
	Non-wild-core	35	11 (31)	24 (69)	12 (34)	12 (34)			
	Gln^{70}	21	5 (24)	16 (76)	8 (38)	8 (38)	0.06	0.04	0.19
	Non-Gln^{70}	47	24 (51)	23 (49)	9 (19)	14 (30)			
	Met^{91}	19	7 (37)	12 (63)	5 (26)	7 (37)	0.59	0.74	0.75
	Non-Met^{91}	49	22 (45)	27 (55)	12 (24)	15 (31)			

SVR = Sustained virological response; ETR = end-of-treatment response; IRRDR = interferon/ribavirin resistance-determining region; Ala^{2360} = alanine at position 2360; ISDR = interferon sensitivity-determining region; Arg^{70} = arginine at position 70; Leu^{91} = leucine at position 91; Gln^{70} = glutamine at position 70; Met^{91} = methionine at position 91.

[a] Total number of isolates with a given factor.
[b] Number of SVR, non-SVR, null-response or relapse (ETR-relapse *plus* breakthrough) cases with a given factor.
[c] Values in parentheses are percentages.

Correlation between Core Polymorphism and Treatment Responses

Recently, it was reported that polymorphism at positions 70 and/or 91 of the core protein of HCV-1b correlates with and predicts the treatment outcome of Japanese patients treated with PEG-IFN/RBV combination therapy [8, 9]. We aimed to test the consistency of this observation among our patient cohort. The result revealed that among 33 patients infected with HCV isolates of wild-core (Arg^{70}/Leu^{91}), 18 (55%), 15 (45%), 5 (15%) and 10 (30%) patients were SVR, non-SVR, null-response and relapse (ETR-relapse *plus* breakthrough), respectively (table 3; fig. 1). On

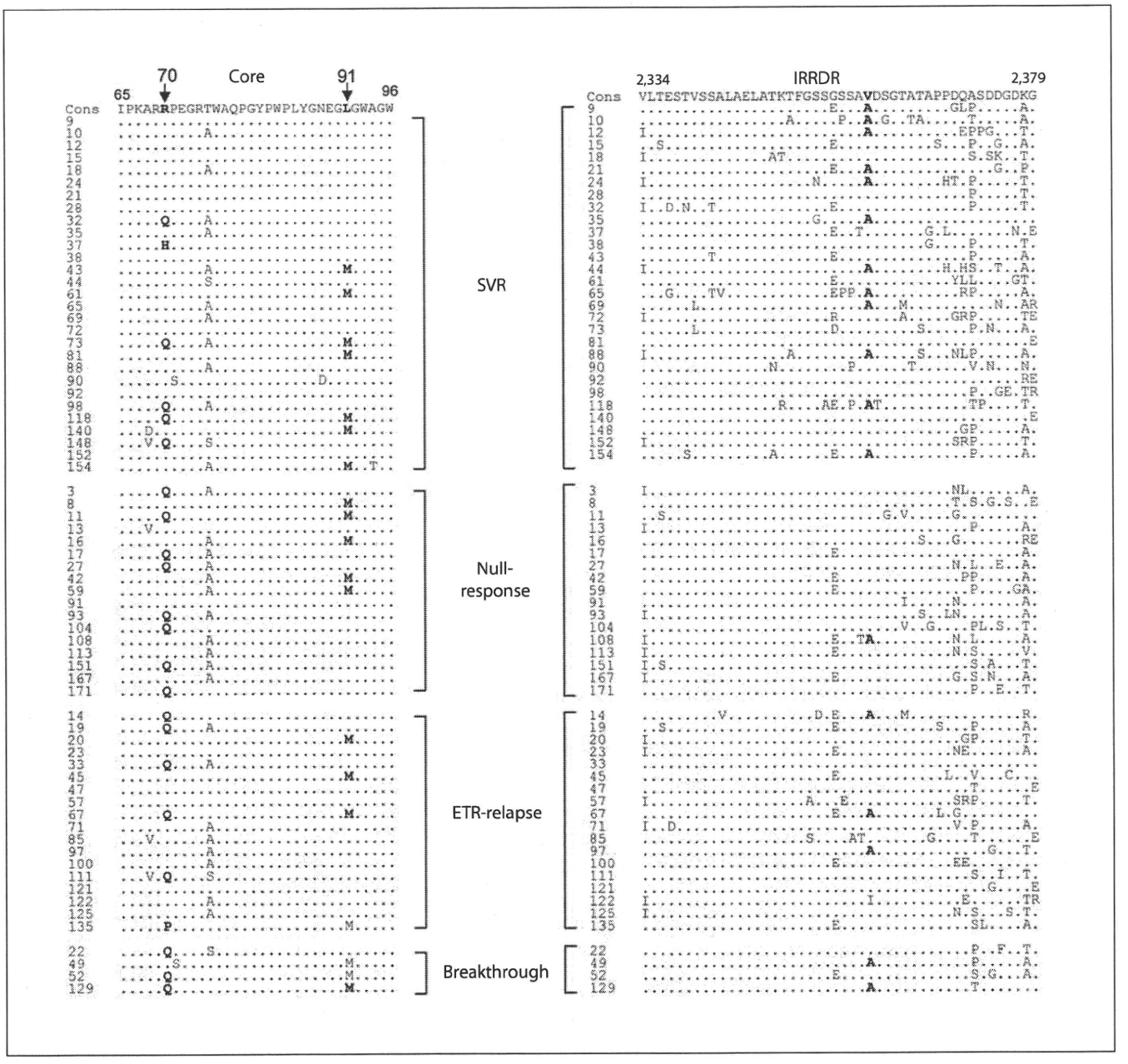

Fig. 1. Sequence alignment of the core protein (aa 65–96) and IRRDR of NS5A obtained from pretreated sera in patients infected with HCV-1b. The consensus (Cons) sequence is shown at the top. Amino acids at positions 70 and 91 of the core protein, and position 2360 of NS5A are shown in boldface.

the other hand, of 35 patients infected with HCV isolates of non-wild-core, 11 (31%), 24 (69%), 12 (34%) and 12 (34%) patients were SVR, non-SVR, null-response and relapse (ETR-relapse *plus* breakthrough), respectively. Thus, there was no significant correlation between wild-core and SVR or non-SVR ($p = 0.1$). However, a single mutation at position 70 (Gln^{70} vs. non-Gln^{70}) was significantly correlated with treatment outcome (SVR vs. null-response; $p = 0.04$).

As for the on-treatment responses, wild-core (Arg^{70}/Leu^{91}) was significantly correlated with EVR and ETR, whereas Gln^{70} was correlated with non-EVR and non-ETR (table 4).

Table 4. Correlation between NS5A and core protein polymorphisms and on-treatment virological responses of patients treated with PEG-IFN/RBV

Protein	Factor	Total[a]	RVR[b]	Non-RVR	EVR	Non-EVR	ETR	Non-ETR	p value		
									RVR vs. non-RVR	EVR vs. non-EVR	ETR vs. non-ETR
NS5A	IRRDR≥6	24	5 (21)[c]	19 (79)	17 (71)	7 (29)	21 (87)	3 (13)	0.12	0.04	0.026
	IRRDR≤5	44	3 (7)	41 (93)	19 (43)	25 (57)	26 (59)	18 (41)			
	Ala^{2360}	18	4 (22)	14 (78)	13 (72)	5 (28)	16 (89)	2 (11)	0.19	0.1	0.04
	Non-Ala^{2360}	50	4 (8)	46 (92)	23 (46)	27 (54)	31 (62)	19 (38)			
	ISDR≥2	18	6 (33)	12 (67)	9 (50)	9 (50)	11 (61)	7 (39)	0.003	0.79	0.39
	ISDR≤1	50	2 (4)	48 (96)	27 (54)	23 (46)	36 (72)	14 (28)			
Core	Wild-core (Arg^{70}/Leu^{91})	33	5 (15)	28 (85)	23 (70)	10 (30)	28 (85)	5 (15)	0.47	0.009	0.009
	Non-wild-core	35	3 (9)	32 (91)	13 (37)	22 (63)	19 (54)	16 (46)			
	Gln^{70}	21	2 (10)	19 (90)	6 (29)	15 (71)	10 (48)	11 (52)	1.0	0.009	0.02
	Non-Gln^{70}	47	6 (13)	41 (87)	30 (64)	17 (36)	37 (79)	10 (21)			
	Met^{91}	19	2 (11)	17 (89)	8 (42)	11 (58)	11 (58)	8 (42)	1.0	0.29	0.25
	Non-Met^{91}	49	6 (12)	43 (88)	28 (57)	21 (43)	36 (73)	13 (27)			

RVR = Rapid virological response; EVR = early virological response; ETR = end-of-treatment response; IRRDR = interferon/ribavirin resistance-determining region; Ala^{2360} = alanine at position 2360; ISDR = interferon sensitivity-determining region; Arg^{70} = arginine at position 70; Leu^{91} = leucine at position 91; Gln^{70} = glutamine at position 70; Met^{91} = methionine at position 91.

[a] Total number of isolates with a given factor. [b] Number of RVR, non-RVR, EVR, non-EVR, ETR or non-ETR cases with a given factor. [c] Values in parentheses are percentages.

Table 5. Correlation between NS5A and core protein polymorphisms

Factor	% (number of subjects/number of subtotal)[a]		p value
	IRRDR≥6	IRRDR≤5	
Ala^{2360}	50 (12/24)	14 (6/44)	0.003
Non-Ala^{2360}	50 (12/24)	86 (38/44)	
ISDR≥2	42 (10/24)	18 (8/44)	0.047
ISDR≤1	58 (14/24)	82 (36/44)	
Wild-core (Arg^{70}/Leu^{91})	67 (16/24)	39 (17/44)	0.04
Non-wild-core	33 (8/24)	61 (27/44)	
Gln^{70}	21 (5/24)	36 (16/44)	0.27
Non-Gln^{70}	79 (19/24)	64 (28/44)	

IRRDR = Interferon/ribavirin resistance-determining region; Ala^{2360} = alanine at position 2360; ISDR = interferon sensitivity-determining region; Arg^{70} = arginine at position 70; Leu^{91} = leucine at position 91; Gln^{70} = glutamine at position 70.

[a] Number of isolates with a certain factor/total number of HCV isolates with IRRDR≥6 or IRRDR≤5.

Correlation between NS5A and Core Polymorphisms

We then examined the possible correlation among the polymorphic factors in NS5A and core proteins. A significant correlation was observed between IRRDR≤5 and non-Ala^{2360} as the majority (86%) of HCV isolates with IRRDR≤5 had non-Ala^{2360} ($p = 0.003$) (table 5). Also, a significant correlation was obtained between IRRDR≤5 and ISDR≤1 since 82% of IRRDR≤5 were ISDR≤1 ($p = 0.047$). When IRRDR and core polymorphisms were compared, IRRDR≥6 was significantly correlated with wild-core (Arg^{70}/Leu^{91}) ($p = 0.04$). On the other hand, there was no significant correlation between IRRDR≥6 and non-Gln^{70}, or IRRDR≤5 and Gln^{70}, although the majority (79%) of IRRDR≥6 were non-Gln^{70}.

Influence of NS5A and Core Polymorphisms on HCV Clearance Kinetics during PEG-IFN/RBV Combination Therapy

To investigate the influence of NS5A and core polymorphisms on HCV-RNA kinetics during the entire course of PEG-IFN/RBV combination therapy, Kaplan-Meier HCV survival curve analysis was carried out based on HCV-RNA positivity according to NS5A and core